Princeton Plasma Physics Laboratory

PPPL- 4368

PPPL- 4368

Effects of Heavy Ions on ULF Wave Resonances Near the Equatorial Region

D.-H.Lee, J.R. Johnson, K. Kim and K.-S.Kim

November, 2008

Prepared for the U.S. Department of Energy under Contract DE-AC02-76CH03073.

Princeton Plasma Physics Laboratory
Report Disclaimers

Full Legal Disclaimer

Trademark Disclaimer

PPPL Report Availability

Princeton Plasma Physics Laboratory:

http://www.pppl.gov/techreports.cfm

Office of Scientific and Technical Information (OSTI):

http://www.osti.gov/bridge

Related Links:

U.S. Department of Energy

Office of Scientific and Technical Information

Fusion Links

Effects of heavy ions on ULF wave resonances near the equatorial region

D.-H. Lee,[1] J. R. Johnson,[2] K. Kim,[3] and K.-S. Kim[1]

J. R. Johnson, Princeton University, Plasma Physics Laboratory, Princeton, NJ 08543.

K. Kim, Division of Energy Systems Research, Ajou University, Suwon 443-749, Korea and Department of Physics, University of Virginia, Charlottesville, Virginia 22904, USA

D.-H. Lee and K.-S. Kim, Department of Astronomy and Space Science, Kyung Hee University, Yongin, Kyunggi, 449-701 Korea. (dhlee@khu.ac.kr)

[1]Department of Astronomy and Space Science, Kyung Hee University, Kyunggi, Korea

[2]Princeton Plasma Physics Laboratory, Princeton, New Jersey, USA.

[3]Division of Energy Systems Research, Ajou University, Kyunggi, Korea

Abstract. Pc1-2 ULF waves are strongly associated with the presence of various ions in the magnetosphere. We investigate the role of heavy ion resonances in nonuniform plasmas near the equatorial region. By adopting the invariant imbedding method, the coupled plasma wave equations are solved in an exact manner to calculate the resonant absorption at the ion-ion hybrid resonance. Our results show that irreversible mode conversion occurs at the resonance, which absorbs the fast wave energy. It is found that waves near the resonances appear with linear polarization, and their amplitude and frequency are sensitive to the properties of the heavy ion plasma composition. We examine how these resonances occur for various $H^+ - He^+$ populations in detail by performing an accurate calculation of the mode conversion efficiency. Because the multi-ion hybrid resonance locations in cold plasmas are determined by simple parameters such as the fraction of the ion number density of each species and the magnetic field, we suggest that it is possible to monitor heavy ion composition by examining the peak frequencies of linearly polarized wave events in either electric field or magnetic field spectral data.

1. Introduction

Pc1-2 waves play an important role in understanding electromagnetic phenomena near the cyclotron frequencies of multi-ion plasmas in space. The presence of heavy ions such as He^+ and O^+ significantly modifies the dispersion relation in the sense that new wave properties arise in the multi-ion plasma, which not present in a single ion plasma. The effect of heavy ions on low frequency dispersion relations was summarized by *Rauch and Roux* [1982] who showed that additional resonances, crossover, and cutoff frequencies involving the multiple ion species are introduced.

Buchsbaum [1960] first introduced the concept that the addition of a second species of heavy ions introduces a resonance (referred to as the Buchsbaum-Bers resonance) where the wavenumber perpendicular to the background magnetic field becomes infinite. This resonance is a principal resonance that occurs in addition to the upper and lower hybrid resonances found in single ion plasmas. He showed that the resonance is associated with the anti-phase motion between two ion species, and the resonance frequency is located between the cyclotron frequencies of the two ions. A new multi-ion resonance is added with each additional ion species. *Smith and Brice* [1964] also showed that for parallel propagation there is a frequency between each pair of ion cyclotron frequencies where the right- and left-hand polarized modes satisfy the same dispersion relation called the crossover frequency. In an inhomogeneous plasma, significant transfer of energy may occur between the right- and left-hand polarized modes near the local crossover frequency near parallel propagation [*Johnson et al.*, 1995].

The dispersion relation of heavy ion waves in the terrestrial magnetosphere has been studied in detail over the last few decades. Observational studies clearly indicate the presence of two ions (H^+ and He^+) and the three ions (H^+, He^+ and O^+) in the wave dispersion. Studies of the observed waves have included ground-based [e.g. *Arnoldy et al.*, 1988; *Engebretson et al.*, 2002] and space-based [e.g. *Anderson et al.*, 1992a, b; *Fraser and Nguyen*, 2001] observational signatures as well as correlation studies based on multi-point measurements [*Bossen et al.*, 1976; *Gendrin et al.*, 1978; *Young et al.*, 1981; *Perraut et al.*, 1984; *Fraser et al.*, 1989]. For instance, the stop bands of He^+ [*Dowden*, 1966; *Fraser*, 1972] and O^+ [*Fraser and McPherron*, 1982; *Inhester et al.*, 1984] have often been used to identify the presence of each heavy ion. The kinetic effects of finite temperature on the generation and propagation of Pc1-2 wave events have also been studied extensively [e.g. *Mauk and McPherron*, 1980; *Mauk et al.*, 1981; *Young et al.*, 1981; *Roux et al.*, 1982; *Gendrin et al.*, 1984; *Kozyra et al.*, 1984; *Horne and Thorne*, 1997; *Summers and Thorne*, 2003].

However, there are some interesting features in satellite observations which still remain unanswered. According to the statistical studies of satellite observations such as *Anderson et al.* [1992a, b] and *Fraser and Nguyen* [2001], it is evident that the wave events near the equatorial region have unique features. One property is that wave events with linear polarization are frequently observed [*Young et al.*, 1981; *Fraser and McPherron*, 1982; *Fraser*, 1985; *Anderson et al.*, 1992b, 1996; *Fraser and Nguyen*, 2001]. The dispersion relation of heavy ions indicates that any branch of the wave mode should be predominantly left-hand (L) or right-hand (R) polarized except for a few exceptions near the crossover frequency or at oblique propagation near the multi-ion hybrid resonances [e.g. *Rauch*

and Roux, 1982; *Fraser*, 1985]. Because wave surveys involve a wide range of observed frequency relative to the ion cyclotron frequency, it is highly unusual that a significant number of wave events are linearly polarized.

Another interesting feature is that the wave properties appear to be sensitive to the local time [e.g. *Anderson et al.*, 1992a, b; *Fraser and Nguyen*, 2001]. For instance, *Anderson et al.* [1992b] shows that the early morning region (AM) is dominated by linearly polarized events, while the noon and dusk region (PM) contain a significant amount of R and L events in addition to the linearly polarized events. The peak frequencies as well as the polarization states are strongly dependent on the local time, which requires an explanation why the AM and PM regions have different characteristics from each other.

It is also known that heavy ions can significantly affect ULF wave phenomena in other planetary environments such as Jupiter (which has a significant source of Iogenic S^{++} and O^+ originating from Io's volcanically generated SO_2 atmosphere). These heavy ions populate the inner Jovian magnetosphere [*Bagenal et al.*, 2004]) and affect low frequency ULF wave propagation in the Io torus [*Glassmeier et al.*, 1989]. Heavy ions should also be important for understanding ULF waves observed at Mercury, which has a significant exospheric source of Na^+ [e.g. *Glassmeier et al.*, 2003, 2004; *Kim et al.*, 2008].

In this study, we solve the full coupled wave equations for wave propagation in a simplified 1D inhomogeneous multi-ion (H^+ and He^+) plasma with parameters typical of the Earth's equatorial magnetosphere near geosynchronous orbit. We first discuss the wave equations and the dispersion relation of heavy ion waves and then introduce the basic properties of wave fields at the heavy ion resonances. In order to solve the coupled full wave equations in a cold plasma limit, we extend a theoretical technique called the in-

variant imbedding method (IIM), which enables us to obtain the resonant absorption in an exact manner without taking a local approximation for the plasma profiles near wave coupling regions. We present the mode conversion at each resonance, which occurs with linear polarization, for various wavenumbers and density population cases. These results suggest that mode conversion at the heavy ion resonances may explain the significant fraction of linearly polarized wave events that have been observed. We also discuss electrostatic and electromagnetic nature of the resonances and the basic properties of both ion and electron resonances in the full wave equations. Finally, we suggest that it may be possible to use wave behavior near heavy ion resonances to monitor heavy ion populations using wave polarization and peak frequency in either electric or magnetic field data.

2. Model and Equations

Previous observations [*Anderson et al.*, 1991, 1992a; *Anderson and Fuselier*, 1993; *Fraser and Nguyen*, 2001] indicate that Pc1-2 waves are found over a broad range of radial distance ($3.5 < L < 10$) in the equatorial magnetosphere. We start with a brief introduction to the dispersion relation of heavy ion plasma and the coupled equations. In order to solve these equation in an exact manner, we extend the invariant imbedding method (IIM), which has recently been developed. Then we introduce the box-like model used in this study, and present case studies for a number of different heavy ion density profiles.

2.1. Dispersion Relation and Wave Equations

The wave equations are derived in general from the following two time-dependent Maxwell's equations,

$$\nabla \times \mathbf{E} = -\frac{\partial \mathbf{B}}{\partial t},$$

$$\nabla \times \mathbf{B} = \mu_o \mathbf{J} + \frac{1}{c^2}\frac{\partial \mathbf{E}}{\partial t} = -\frac{i\omega}{c^2}\epsilon \cdot \mathbf{E}, \tag{1}$$

which can be written as by either $\mathbf{E}$ or $\mathbf{B}$ by assuming $e^{-i\omega t}$:

$$\nabla \times (\nabla \times \mathbf{E}) = \frac{\omega^2}{c^2}\epsilon \cdot \mathbf{E} = 0, \tag{2}$$

$$\nabla \times (\epsilon^{-\mathbf{1}} \cdot \nabla \times \mathbf{B}) = \frac{\omega^2}{c^2}\mathbf{B} \tag{3}$$

where c is the speed of the light and ϵ is the dielectric tensor in a plasma. In a cold fluid plasma where the magnetic field is assumed to be constant ($\mathbf{B_o} = B_o\hat{z}$), the dielectric tensor and the Stix tensor elements S, D and P are given by

$$\epsilon = \begin{pmatrix} S & -iD & 0 \\ iD & S & 0 \\ 0 & 0 & P \end{pmatrix},$$

$$\begin{aligned} S &= 1 - \sum_j \frac{\omega_{pj}^2(\omega + i\nu)}{\omega\left\{(\omega + i\nu)^2 - \omega_{cj}^2\right\}}, \\ D &= \sum_j \frac{\omega_{pj}^2\omega_{cj}}{\omega\left\{(\omega + i\nu)^2 - \omega_{cj}^2\right\}}\alpha_j \left(\alpha_j = \frac{q_j}{|q_j|}\right), \\ P &= 1 - \sum_j \frac{\omega_{pj}^2}{\omega(\omega + i\nu)}, \end{aligned} \tag{4}$$

where ω_{pj}, ω_{cj} and q_j are the plasma frequency, cyclotron frequency and charge of j-th species, and ν is the collision frequency of the medium.

In a uniform plasma, if the wavevector is assumed to be $\mathbf{k} = k_\perp\hat{x} + k_\parallel\hat{z} = k(\sin\theta\hat{x} + \cos\theta\hat{z})$, the dispersion relation in terms of the refraction indices $n = kc/\omega$,

$n_\parallel = k_\parallel c/\omega$ and $n_\perp = k_\perp c/\omega$ is given by

$$\tan^2\theta = \frac{n_\perp^2}{n_\parallel^2} = -\frac{P(n^2-R)(n^2-L)}{(Sn^2-RL)(n^2-P)}. \quad (5)$$

where $R = S + D$ and $L = S - D$. In general, the condition of resonances is satisfied when n goes to infinity: either $n_\perp \to \infty$ or $n_\parallel \to \infty$. In both cases, (5) becomes $\tan^2\theta = -P/S$. If we assume that inhomogeneity lies in the x direction perpendicular to the background magnetic field, the resonance would occur when $n_\perp$ ($k_\perp$) goes to infinity, which is equivalent to $S = 0$. In the single ion case, the condition $S = 0$ has only two resonances: the upper hybrid resonance, which is associated primarily with the motion of electrons, and the lower hybrid resonance, which involves a combined motion of both electrons and ions (in phase). However, in the multi-ion case, an resonances (Buchsbaum-Bers) appear for each new species of ion, which is associated with the out-of-phase (or in-phase) motion among the different ions. It should also be noted that for field-aligned propagation, the location S=0 also corresponds to a cutoff condition for a refracted wave packet and and leads to wave reflection and bouncing wave packets between S=0 locations. Mode conversion for field-aligned propagation has been discussed elsewhere [e.g. *Johnson et al.*, 1995; *Johnson and Cheng*, 1999].

Under a reasonable assumption of $\omega_{pe} \gg \omega_{ce}$ in space, the Buchsbaum-Bers resonance frequency (ω_{bb}) for two ions ($i = 1, 2$) is approximated as

$$\omega_{bb}^2 = \omega_{c1}\omega_{c2}\frac{\omega_{c2}A_1 + \omega_{c1}A_2}{\omega_{c1}A_1 + \omega_{c2}A_2}, \quad (6)$$

where $A_j = n_j/n_e$ the fraction of the ion density occupied by the jth ion species and $n_e = n_1 + n_2$ is the electron density. It should be noted that ω_{bb} is determined only by the magnetic field (easily measured) and the relative population of each ion species,

which constrains the background ion composition if the location of the resonance can be identified through wave observations.

When the frequency is below the ion cyclotron frequency and electron inertial effects are ignored ($Sn_\perp^2 \ll Pn_\parallel^2$ and $RL = S^2 - D^2 \ll PS$) in the dispersion relation, it is possible to derive a simplified the dispersion relation for perpendicular propagation of compressional waves can be approximated as

$$n_\perp^2 \approx \frac{(L - n_\parallel^2)(R - n_\parallel^2)}{(S - n_\parallel^2)}. \tag{7}$$

This approximate dispersion relation has a resonance when when $n_\perp \to \infty$ (where the approximation obviously breaks down). This resonance is referred to as the ion-ion (bi-ion) resonance which occurs at the frequency, ω_{ii}, determined from $S = n_\parallel^2$ in (7), which corresponds to the Alfven resonance in the low frequency limit ($\omega \ll \omega_{cj}$) such as in MHD. The relationship between the Buchsbaum-Bers resonance and the ion-ion hybrid resonance will be discussed later in Discussion 4.2.

In an inhomogeneous plasma where we assume one-dimensional inhomogeneity in the radial direction (x) near the equatorial region, the plasma wave equations are given by two dependent variables, which satisfy two second-order coupled differential equations. When $\mathbf{B} = B_o\hat{z}$ and $\mathbf{k}_\parallel = k_\parallel\hat{z}$ is assumed, the dependence on z of all wave functions can be taken as being through a factor $e^{ik_\parallel z}$. Then, after straightforward calculations from Maxwell's equation (1), we have two coupled equations in terms of E_y and B_y as follows:

$$\frac{d^2\psi}{dx^2} - \frac{d\mathcal{E}(x)}{dx}\mathcal{E}^{-1}(x)\frac{d\psi}{dx} + \frac{\omega^2}{c^2}\mathcal{E}(x)\mathcal{M}(x)\psi = 0\ , \tag{8}$$

where

$$\psi = \begin{pmatrix} E_y \\ cB_y \end{pmatrix},$$

$$\mathcal{E} = \begin{pmatrix} 1 & 0 \\ 0 & P(x) \end{pmatrix},$$
$$\mathcal{M} = \begin{pmatrix} \frac{S^2(x)-D^2(x)}{S(x)} - \frac{c^2k_\parallel^2}{\omega^2} & i\frac{ck_\parallel D(x)}{\omega S(x)} \\ -i\frac{ck_\parallel D(x)}{\omega S(x)} & 1 - \frac{c^2k_\parallel^2}{\omega^2 S(x)} \end{pmatrix} \tag{9}$$

Here $\mathcal{EM}$ is given by

$$\mathcal{EM} = \begin{pmatrix} \frac{S^2(x)-D^2(x)}{S(x)} - \frac{c^2k_\parallel^2}{\omega^2} & i\frac{ck_\parallel D(x)}{\omega S(x)} \\ -i\frac{ck_\parallel D(x)}{\omega S(x)} P & \left[1 - \frac{c^2k_\parallel^2}{\omega^2 S(x)}\right] P \end{pmatrix}. \tag{10}$$

On the plane of incidence (xz- plane), E_y and B_y represent TE and TM modes in vacuum in the sense that they are normal to the plane of incidence, respectively. It is sometimes useful, for convenience, to renormalize (10) by multiplying rows of by a factor. For instance, in the uniform region marked by "1", where the Stix elements are denoted by S_1, D_1 and P_1, we change $\mathcal{E}$ and $\mathcal{M}$ with the wave equation unchanged as follows:

$$\mathcal{E} = \begin{pmatrix} 1 & 0 \\ 0 & \frac{P(x)}{P_1} \end{pmatrix},$$
$$\mathcal{M} = \begin{pmatrix} \frac{S^2(x)-D^2(x)}{S(x)} - \frac{c^2k_\parallel^2}{\omega^2} & i\frac{ck_\parallel D(x)}{\omega S(x)} \\ -i\frac{ck_\parallel D(x)}{\omega S(x)} P_1 & \left[1 - \frac{c^2k_\parallel^2}{\omega^2 S(x)}\right] P_1 \end{pmatrix}. \tag{11}$$

In this study, we will solve (8) with $\mathcal{E}(x)$ and $\mathcal{M}(x)$ given by (11) in an exact manner without making any local approximations for the tensor elements.

2.2. Invariant Imbedding Equations

The invariant imbedding method (IIM) is a well known tool that has been used for solving transport equations in many research areas such as radiation transfer [*Chandrasekhar*, 1960], optical electromagnetic waves [*Klyatskin*, 1994], electron localization in solids [*Rammal and Doucot*, 1987], ocean waves [*Klyatskin et al.*, 1998], compressional MHD wave [*Lee et al.*, 2002], and Langmuir waves in unmagnetized plasmas [*Kim and Lee*, 2005]. This method enables us to focus on the exact reflection and transmission rather than the details about local properties inside the inhomogeneous medium [*Bellman*

and Wing, 1992], which can provide a powerful tool in determining the mode conversion rate in complicated inhomogeneous plasmas [*Lee et al.*, 2002; *Kim and Lee*, 2005].

Recently, *Kim et al.* [2005] generalized the invariant imbedding theory of wave propagation and derived new invariant imbedding equations for the propagation of an arbitrary number of *coupled* waves of any kind in arbitrarily inhomogeneous stratified media, where the wave equations are effectively one-dimensional. They established the validity and the usefulness of their results by applying this method to the propagation of circularly polarized electromagnetic waves in one-dimensional photonic crystal chiral media. It has also been demonstrated that this new version of IIM is very useful in solving the coupled plasma wave equations in a one-dimensional inhomogeneous medium [*Lee et al.*, 2006; *Kim and Lee*, 2006]. We adopt this method in this study to solve the wave scattering/asorption problem for waves propagating in an inhomogeneous, multi-ion plasma. According to *Kim and Lee* [2006], the equation (8) may be solved by adopting the invariant imbedding equations, which enables us to efficiently calculate the matrix reflection and transmission coefficients inside the inhomogeneous media without making any local approximations to simplify the differential equation.

We assume that the inhomogeneous medium of thickness X lies in $0 \leq x \leq X$ between two uniform regions, where both $\mathcal{E}$ and $\mathcal{M}$ are functions of x. We assume that the waves are incident from the right (Region 1) where $x > X$ and transmitted to the left (Region 2) where $x < 0$ in all subsequent calculations [*Lee et al.*, 2002]. For convenience, the wave equation (8) can be transformed as follows, which is derived in Appendix A.

$$\frac{d^2\Phi}{dx^2} - \frac{d\tilde{\mathcal{E}}(x)}{dx}\tilde{\mathcal{E}}^{-1}(x)\frac{d\Phi}{dx} + \tilde{\mathcal{E}}(x)H^2\tilde{\mathcal{M}}(x)\Phi = 0 \tag{12}$$

where $\tilde{\mathcal{E}}$ and $\tilde{\mathcal{M}}$ are defined in Appendix A, and

$$\Phi(x) = \begin{pmatrix} \Phi_{11} & \Phi_{12} \\ \Phi_{21} & \Phi_{22} \end{pmatrix}. \tag{13}$$

Each component of Φ_{ij} in (13) represents the i-th component when the j-th component is an incident wave. Thus the first column of the matrix Φ represents the wave functions when the first eigenstate wave is incident, and the second column represents the wave functions when the other eigenstate wave is incident.

Since the waves are incident from Region 1 where $x > X$ and transmitted to Region 2 where $x < 0$, we have the wave functions in the two uniform regions as follows:

$$\begin{cases} e^{-iH(x-X)} + e^{iH(x-X)} r(X) & \text{if } x > X \\ e^{-iQx} t(X) & \text{if } x < 0 \end{cases} \tag{14}$$

where H and Q are diagonal matrices satisfying $H_{ij} = h_i \delta_{ij}$ and $Q_{ij} = q_i \delta_{ij}$ where h_i and q_i are the x component wavenumbers in Region 1 and Region 2, respectively, for the ith wave as shown in Appendix A. The multi-ion plasma eigenmodes in uniform plasmas are discussed in detail by [*Andre*, 1985].

The reflection and the transmission coefficients should satisfy the following first-order differential equations, respectively, which are derived by *Kim and Lee* [2006],

$$\frac{dr}{dX} = i\Big[r(X)\tilde{\mathcal{E}}(X)H + \tilde{\mathcal{E}}(X)Hr(X)\Big] - \frac{i}{2}\Big[r(X)+I\Big]\Big[\tilde{\mathcal{E}}(X)H - H\tilde{\mathcal{M}}(X)\Big]\Big[r(X)+I\Big], \tag{15}$$

$$\frac{dt}{dX} = i\,t(X)\tilde{\mathcal{E}}(X)H - \frac{i}{2}t(X)\Big[\tilde{\mathcal{E}}(X)H - H\tilde{\mathcal{M}}(X)\Big]\Big[r(X)+I\Big]. \tag{16}$$

The IIM provides a tool to calculate how the coefficients change when the barrier's width, X, changes. We solve the first-order differential equations (15,16) numerically, using

appropriate initial conditions and obtain the reflection and transmission coefficients as functions of X. The invariant imbedding equations should satisfy the following initial conditions at $X = 0$:

$$r(0) = C_2 t(0) - I$$
$$t(0) = 2\Big(C_2 + H^{-1} C_2 Q\Big)^{-1}. \tag{17}$$

where C_2 the linear transformation matrix from the plasma wave eigenstates of Region 2 to the eigenstates of Region 1. The derivation is presented in detail in Appendix A.

Reflectivity R, transmissivity T and absorption A are given by

$$\begin{aligned} R_{ij} &= \frac{h_i}{h_j}|r_{ij}|^2, \quad T_{ij} = \frac{q_i}{h_j}|t_{ij}|^2, \\ A_j &= 1 - (R_{1j} + R_{2j} + T_{1j} + T_{2j}) \end{aligned} \tag{18}$$

where i denotes a reflected or transmitted wave component and j denotes an incident wave component. This absorption is associated with the loss of incident energy flow, and results either from resonant absorption or dissipation while the waves as they propagate through the inhomogeneous region. We will consider the absorption of the fast compressional wave in this study.

2.3. Models

In this study, we consider the region near the geostationary orbit ($L = 6.6$), for convenience, which tends to have abundant Pc1-2 activity. A 1D box-like model is assumed with parameters representative of the equatorial magnetosphere. In order to focus on how variations in the heavy ion population affect the propagation of Pc1-2 waves, we assume that the background magnetic field is constant ($\mathbf{B_o} = B_o \hat{z}$) and the total number density of ions is constant. Thus the magnetic field intensity is given by $B_o = 0.31 \times 10^{-4}/6.6^3 T \simeq 108 nT$.

The number densities, cyclotron frequencies, plasma frequencies of the j-th species of charged particles are given by n_j, f_{cj} and f_{pj}, and so on. For instance, when $n_H = 10/cm^3$, $f_{cH} = 1.65Hz$ and $f_{pH} = 662.6Hz$ for protons, respectively. The electron density is equal to the total ion density ($n_e = \Sigma n_j$).

In this paper, we consider the two-ion plasma consisting of H^+ and He^+ with various ion density profiles. First, two different types of density profiles are examined: step-like and bump-like cases. For each profile, we consider how mode conversion depends on wavenumber and gradient scale of the background density. Second, we compare our mode conversion calculations with the mode conversion in Budden's problem. Third, the effect of total plasma density on the mode conversion process is examined over a range $n_e = 0.5 - 10^3/cm^3$ characteristic of plasma sheet→plasmasphere. Finally, it is shown how the relative abundance of heavy ions affects the mode conversion.

In addition to the cases mentioned above, we also examine each case when n_H and n_{He} are switched, which corresponds to a reversal of heavy ion density gradient.

3. Mode Conversion at Resonances

Figure 1 shows the density models of H^+ and He^+, where the box has a scale of $X = 1R_E$ in the radial direction. The total density is constant as $n_e = n_H + n_{He} = 10/cm^3$, but the relative ion population is assumed to vary significantly. In order to focus on the importance of the heavy ion concentration, we assume a large composition variation in this model. Each density variation is given by almost 100% of the total density in Figure 1a. For instance, n_H/n_e (dotted line) varies from 0.999 to 0.001 when n_{He}/n_e (dashed line) varies from 0.001 to 0.999. The density variation becomes step-like over the different gradient scales marked by (1, 2, 3) which are given by $\Lambda = 0.2$, 0.5 and $1.0R_E$, respectively. Since

the incident wave is from Region 1 of $x > X$, the propagation is from a H^+-rich plasma to a He^+-rich plasma. In Figure 1b, a bump-like He^+ density variation is prescribed where n_{He}/n_e (dashed line) varies from 0.001 to 0.3 with the maximum density located in the middle of the crest. The gradient scales (1, 2, 3) here are given by 0.4, 1.0 and $2.0R_E$, respectively. We assume that fast compressional waves are incident radially inward from the right side ($x > X$) of the box.

In addition to the profiles in Figure 1, we also examine each case when n_H and n_{He} are switched. Then, in the step-like profile of Figure 1a, the incident wave is from He^+-rich plasma to H^+-rich plasma. In the bump-like profile of Figure 1b, the bump is assumed in the H^+ density.

3.1. Dependence on Gradient Scales and Wavenumbers

Figure 2 shows the resonance frequency profile and the resonant absorption when the ion densities are given by Figure 1a. The left column of Figure 2 shows the frequency profiles of Buchsbaum-Bers and ion-ion hybrid resonances for different $k_\parallel = 2\pi/\lambda_\parallel$. As the density variation in Figure 1a is monotonic in a step-like profile, the resonance frequency also becomes monotonic. Since f_{bb} ($= \omega_{bb}/2\pi$) is determined only by B and the relative ion composition ratio as shown in (6), it remains the same for different $\lambda_\parallel$. However, the condition of the ion-ion hybrid resonance, $S = n_\parallel^2$, should depend on $k_\parallel$, and the resonance frequency becomes different for three values of $\lambda_\parallel$. For relatively large $\lambda_\parallel$ ($\geq 1R_E$), the resonance frequencies are almost identical, but become slightly different as $\lambda_\parallel$ decreases.

The right column of Figure 2 shows the resonant absorption A defined in Section 2.2, which is calculated using the invariant imbedding equations. When $\lambda_\parallel$ varies over 0.3 to $2.0R_E$, the absorption maximizes around 0.25 at both edges near each ion cyclotron

frequency. The first peak is located near $f_{cHe} = 0.25 f_{cH}$, and the second peak is near f_{cH}. Since the resonance frequency given by (6) gets close to f_{cHe} (f_{cH}) in the H-He plasma only if n_{He}/n_e (n_H/n_e) becomes 0, Figure 2 shows that the resonant absorption becomes significant only when the plasma has a very small abundance of either ion species. The first peak near f_{cHe} occurs where the local n_{He} population is only a few percent, and the second peak near f_{cH} occurs where the local n_H population is only a few percent.

The resonant absorption in Figure 2 shows that the mode conversion efficiency is not very sensitive to the field-aligned wavenumber over the range, $\lambda_\parallel = 0.3 - 2.0 R_E$, which reasonably fits the scale of Pc1-2 pulsations. The absorption feature remains the same even for the larger $\lambda_\parallel$ in unpublished calculations. For relatively short wavelength $\lambda_\parallel = 0.3 R_E$ in Figure 2a, the absorption range becomes only slightly extended compared to the cases of larger wavelengths in Figure 2b and 2c. However, Figure 2 does suggest that the resonant absorption strongly depends on the gradient scales. The frequency range of resonant absorption widens as the gradient scale becomes smaller (from 3 to 1) becoming widest for a sharp gradient.

When n_H and n_{He} are switched (in the profiles of Figure 1a), Figure 3 shows that the resonance frequency now decreases in the direction of the incident wave propagation, and the resonant absorption becomes greatly enhanced, which reaches 1.0. It indicates that the wave propagating from He^+-rich to H^+-rich plasma becomes significantly absorbed into the resonance over a wide range of frequencies except for the nearby edges close to each ion cyclotron frequency. If the two absorption profiles in Figures 2 and 3 are compared with each other, they tend to be opposite to each other in terms of the peak

locations and the dependence on gradient scales, even though the absorption peak values are different with 0.25 and 1.0, respectively.

Figure 4 shows the case of the bump-like profiles presented in Figure 1b. As the density variation of n_{He} in Figure 1b has a crest, the resonance frequency is also bump-like. The mode conversion rate is not so sensitive to the field-aligned wavelength again as shown in Figures 2 and 3. However, the absorption peaks in Figure 3 are found to reach about 0.5, which double the absorption of Figure 2. In addition, the frequency range of absorption appears with a single peak near the lower range, which becomes close to f_{cHe} for weaker gradients. The absorption frequency range tends to broaden for sharper gradients, which is consistent with the results of the step-like cases in Figure 2.

Figure 5 shows the resonant absorption when n_H and n_{He} are switched in Figure 1b, which corresponds to the bump-like density profile of H^+. Now the resonance frequency has a well. The absorption is nearly complete (1.0) as in Figure 3 over most frequencies lying within the resonance band for all three gradient scales. However, it is interesting to note that the absorption has some spiky variations near f_{cH} with an harmonic feature, which drops down to about 0.5.

3.2. Mode Conversion Efficiency

In the results presented above, we solved the full wave equations including both fast ion waves and electron inertial waves in the cold plasma limit. However, our results are mainly associated with the ion waves, which have relatively large wavelength such that thermal are often negligible. In the cold plasma limit, it is well known that the absorption of the fast wave can be approximated as Budden problem [*Budden*, 1985; *Swanson*, 1985] in many cases [e.g. *Ngan and Swanson*, 1977; *Perkins*, 1977; *Swanson*, 1985; *Ram et al.*,

1996]. In this section, we adopt this approximation and examine the properties of mode conversion efficiency above in terms of a simple Budden problem.

If $n_\perp$ is calculated from (5) in a uniform plasma, we have

$$n_\perp^2 = \frac{1}{2S}(\alpha \pm \beta) \tag{19}$$

where

$$\begin{aligned} \alpha &= (P+S)\delta - D^2 \\ \beta &= \sqrt{\alpha^2 + 4PS(D+\delta)(D-\delta)} \\ \delta &= S - n_\parallel^2. \end{aligned} \tag{20}$$

At frequencies below the ion gyrofrequency, these two modes are characterized by two different spatial scales corresponding to electron waves with large $n_\perp$ (with spatial scale of the electron skin depth) and ion waves with small $n_\perp$ (with spatial scale on the order of V_A/f), respectively. The different role of electrons and ions is examined and discussed in detail later in Section 4.2, where we discuss how the Buchsbaum-Bers resonance and ion-ion hybrid resonance are associated with electron and ion effects in the dispersion relation. If we apply the same assumption of $Sn_\perp^2 \ll Pn_\parallel^2$ and $RL = S^2 - D^2 \ll PS$ for the ion-ion hybrid resonance when the effect of electron inertia becomes less important, we can expand (19) in terms of $|P\delta| \gg 1$ as follows:

$$\begin{aligned} 2Sn_\perp^2 \;&\approx\; (P+S)\delta - D^2 \\ &\pm\; |P\delta|\left[1 + \frac{S\delta - D^2}{P\delta} + \frac{2S(D^2-\delta^2)}{P\delta^2}\right]. \end{aligned} \tag{21}$$

Whether $P\delta$ is positive or negative, the solution of small $n_\perp$ is reduced to

$$n_\perp^2 \approx \frac{\delta^2 - D^2}{\delta} = \frac{(L - n_\parallel^2)(R - n_\parallel^2)}{(S - n_\parallel^2)}, \tag{22}$$

which corresponds to the dispersion relation presented in (7).

To approximate the solutions near the resonance in an inhomogeneous plasma, we assume linear profiles in x from the Taylor expansion such as

$$\begin{aligned} \delta &\approx \kappa x \\ \Delta &\equiv \delta^2 - D^2 \approx \kappa_c (x - a) \end{aligned} \tag{23}$$

where $x = 0$ and $x = a$ are the location of resonance and cutoff, respectively. Then (22) becomes

$$n_\perp^2 \approx \frac{\kappa_c (x - a)}{\kappa x} = \frac{\kappa_c}{\kappa} \left(1 - \frac{a}{x}\right), \tag{24}$$

which is equivalent to the Budden equation:

$$\frac{d^2 y}{dx^2} + k_0^2 \left(1 - \frac{a}{x}\right) y = 0 \tag{25}$$

where $k_0^2 = \kappa_c / \kappa$ and x is the normalized coordinate obtained by multiplying ω/c.

Since κ and κ_c in (23) satisfy $\delta' = S' = \kappa$ and $\Delta' = \kappa_c$, we have the following relations near the resonance

$$\begin{aligned} k_0^2 &= \frac{\Delta'}{\delta'} \\ a &= -\frac{\Delta}{\kappa_c} = -\frac{\Delta}{\Delta'}. \end{aligned} \tag{26}$$

This relation is equivalent to the expression previously derived by *Jacquinot et al.* [1977]

$$\begin{aligned} k_0^2 &= \frac{\frac{d}{dx}(L - n_\parallel^2)(R - n_\parallel^2)}{\frac{d}{dx}(S - n_\parallel^2)} \\ a &= -\frac{(L - n_\parallel^2)(R - n_\parallel^2)}{\frac{d}{dx}(L - n_\parallel^2)(R - n_\parallel^2)}. \end{aligned} \tag{27}$$

In Appendix B, we derive the expression for $k_0 a$ in our model where the background magnetic field and the electron density are assumed to be constant and gradients are only due to variation in ion concentration.

As derived in Appendix B, $k_0 a$ satisfies

$$|k_0 a| \propto \omega^{5/2} \mid \frac{1}{n'_{He}} \frac{n_e^{3/2}}{\sqrt{(4f_1 - f_2)(f_2 - 16f_1)}} \mid \tag{28}$$

where

$$\begin{aligned} f_1 &= \frac{1}{1 - Y_H^2} \\ f_2 &= \frac{1}{1 - Y_{He}^2} \\ Y_j &= \omega_{cj}/\omega. \end{aligned} \tag{29}$$

In general, $|k_0 a|$ tends to remain relatively large, but (28) suggests that it can be significantly reduced to a small value only if i) the total electron density n_e becomes relatively small, ii) the density gradient n'_{He} becomes large, or iii) the frequency becomes close to either ω_{cH} ($f_1 \to \infty$) or ω_{cHe} ($f_2 \to \infty$). In fact, the relation (28) based on the Budden problem is consistent with many features in Figures 2-5.

When the incident wave propagates from a H^+-rich to a He^+-rich plasma region with a monotonic density variation like the step-like profile in Figure 1a, the Budden equation in (25) has a $k^2(x)$ profile topologically equivalent to the profile shown in Figure 6a. The wave propagates from the right to left region, meets the cutoff point at $x = a$ and the resonance at $x = 0$ in time. When n_H and n_{He} are switched, the incident wave propagates from He^+-rich to H^+-rich plasma and $k^2(x)$ should have a reflected profile with respect to the y axis. Then the problem becomes equivalent to the case that the incident wave propagates from the left region in Figure 6a. In the Budden problem, it is well known that the reflection and transmission coefficients are

$$\begin{aligned} T_I &= e^{-\eta} \\ R_I &= -(1 - e^{-2\eta}) \end{aligned}$$

$$A_I = 1 - R_I^2 - T_I^2 = e^{-2\eta}(1 - e^{-2\eta})$$
$$\eta = \frac{\pi k_0 a}{2} \tag{30}$$

for case where the wave propagates from a H^+-rich to a He^+-rich plasma, and

$$T_{II} = e^{-\eta}$$
$$R_{II} = 0$$
$$A_{II} = 1 - R_{II}^2 - T_{II}^2 = 1 - e^{-2\eta} \tag{31}$$

when the wave propagates from a He^+-rich to a H^+-rich plasma.

The absorption in the first case can reach a peak value of $A_I(max) = 0.25$ when $e^{-2\eta} = 0.5$ or $k_0 a = ln2/\pi \approx 0.22$. When η or $k_0 a$ becomes either significantly large or small, the absorption, A_I, becomes negligible. This result explains several features shown in Figure 2. First, it explains why the peak value reaches 0.25 because $A_I(max) = 0.25$. It also explains why the absorption peak occurs near either ω_{cH} or ω_{cHe} because $k_0 a$ in (28) can only be small enough to give maximum absorption (0.22) if $\omega \approx \omega_{cH}$ ($f_1 \to \infty$) or $\omega \approx \omega_{cHe}$ ($f_2 \to \infty$) as noted in condition iii) earlier. Finally, condition ii) explains why mode conversion becomes more efficient over a broader range when the density gradients become sharper because $k_0 a$ is proportional to the gradient scale length.

For the second case where the incident wave propagates from a He^+-rich to a H^+-rich plasma, the wave can reach the resonance region directly without cutoff, and no reflected waves exist. For this case, when $\eta \gg 1$ $A_{II}(max) = 1.0$, in contrast to the previous case where the wave approaches the resonance through the evanescent region. This result explains why the absorption is found to be perfect over a broad range of frequencies in Figure 3 where conditions i), ii) and iii) for small $k_0 a$ are not satisfied. It is also interesting

to note that the absorption becomes less effective when the gradient becomes large, which reduces $k_0 a$ (condition iii).

3.3. Effects of Multiple Resonances

When the density variation is no longer monotonic and has a bump-like or well-like profile, resonances occur at multiple locations where the wave frequency matches the resonance condition. Since both reflection and transmission occur at each resonance, the addition of resonances affects the total mode conversion efficiency which will involve transmitted and reflected waves propagating in the additional layer between the two neighboring resonances.

The bump-like enhancement of n_{He} in Figure 1b allows the same type of f_{bb} as shown in Figure 4. For a given frequency, the resonance can occur at the two locations on each side. When the incident wave propagates from H^+-rich to He^+-rich plasma region like in Figure 1b, Figure 6b shows the case of two resonances, which occur in our bump-like n_{He} distribution. Since reflection and transmission should depend on the direction of propagation, it can be approximated by a three-layered problem marked by 1, 2, and 3, respectively in Figure 6b.

If we define $\hat{r}_{ij}$ and $\hat{t}_{ij}$ as the reflection and transmission coefficients at each boundary when the wave propagates from the j-th layer to i-th layer, total reflection and transmission coefficients can be written in terms of $\hat{r}_{ij}$ and $\hat{t}_{ij}$:

$$\begin{aligned}
\hat{r} &= \hat{r}_{21} + \hat{t}_{21}\hat{r}_{32}\hat{t}_{12}e^{i\hat{\beta}}\left[1 + \hat{r}_{12}\hat{r}_{32}e^{i\hat{\beta}} + \left(\hat{r}_{12}\hat{r}_{32}e^{i\hat{\beta}}\right)^2 + \ldots\right] \\
&= \hat{r}_{21} + \frac{\hat{t}_{21}\hat{r}_{32}\hat{t}_{12}e^{i\hat{\beta}}}{1 - \hat{r}_{12}\hat{r}_{32}e^{i\hat{\beta}}} \\
\hat{t} &= \hat{t}_{21}\hat{t}_{32}e^{i\frac{\hat{\beta}}{2}}\left[1 + \hat{r}_{12}\hat{r}_{32}e^{i\hat{\beta}} + \left(\hat{r}_{12}\hat{r}_{32}e^{i\hat{\beta}}\right)^2 + \ldots\right]
\end{aligned}$$

$$= \frac{\hat{t}_{21}\hat{t}_{32}e^{i\frac{\hat{\beta}}{2}}}{1-\hat{r}_{12}\hat{r}_{32}e^{i\hat{\beta}}}. \quad (32)$$

In case of the propagation from H^+-rich to He^+-rich region in Figure 1b, $\hat{r}_{ij}$ and $\hat{t}_{ij}$ are:

$$\begin{aligned}
\hat{t}_{21} &= T_0 = e^{-\eta} \\
\hat{r}_{21} &= R_0 = -(1-e^{-2\eta}) \\
\hat{t}_{32} &= T_1 = e^{-\eta} \\
\hat{r}_{32} &= R_1 = 0 \\
\hat{t}_{12} &= T_2 = e^{-\eta} \\
\hat{r}_{12} &= R_2 = 0, \quad (33)
\end{aligned}$$

where we can assume that η at the two resonances is the same because of symmetry $k^2(x) = k^2(-x)$. From (32) and (33), we obtain

$$\begin{aligned}
\hat{r} &= -(1-e^{-2\eta}) \\
\hat{t} &= e^{-2\eta}e^{\frac{i\hat{\beta}}{2}} \\
A &= 1-|\hat{r}|^2-|\hat{t}|^2 = 2e^{-2\eta}(1-e^{-2\eta}) \quad (34)
\end{aligned}$$

where A has a maximum of 0.5 at $e^{-2\eta} = 0.5$. The maximum absorption increases by a factor of 2 at the same η compared to that of the step-like case. The transmitted wave after the first resonance is absorbed again at the second resonance with each amount of 0.25, respectively. In this case, the effect of multiple reflections inside region 2 in Figure 6b disappears because $\hat{r}_{32} = 0$ at the second resonance. This result explains why the absorption peak can reach 0.5 in Figure 4. The dependence on the gradient scale is also consistent with the prediction of (28), which shows that the absorption becomes small when the gradient becomes zero near the top of the bump.

When n_H and n_{He} are switched and the incident wave propagates from a He^+-rich to a H^+-rich plasma in Figure 6b, the resonance frequency profile becomes well-like in Figure 5. In this case, the $k^2(x)$ profile is reflected about $k^2(x) = k_o^2$ (shown as a dotted line in Figure 6b). Then all coefficients should be changed as follows:

$$\begin{aligned}
\hat{t}_{21} &= T_0 = e^{-\eta} \\
\hat{r}_{21} &= R_0 = 0 \\
\hat{t}_{32} &= T_1 = e^{-\eta} \\
\hat{r}_{32} &= R_1 = -(1 - e^{-2\eta}) \\
\hat{t}_{12} &= T_2 = e^{-\eta} \\
\hat{r}_{12} &= R_2 = -(1 - e^{-2\eta}).
\end{aligned} \tag{35}$$

From (32), we have the total reflection and transmission coefficients:

$$\begin{aligned}
\hat{r} &= \frac{-\xi(1-\xi)e^{i\hat{\beta}}}{1-(1-\xi)^2 e^{i\hat{\beta}}} \\
\hat{t} &= \frac{\xi e^{i\frac{\hat{\beta}}{2}}}{1-(1-\xi)^2 e^{i\hat{\beta}}} \\
A &= 1 - |\hat{r}|^2 - |\hat{t}|^2 \\
&= 1 - \frac{(1+\zeta^2)(1-\zeta)^2}{1+\zeta^4 - 2\zeta^2 \cos\hat{\beta}}
\end{aligned} \tag{36}$$

where

$$\begin{aligned}
\xi &= e^{-2\eta} \\
\zeta &= 1 - \xi^2 = 1 - e^{-4\eta} \\
\hat{\beta} &\approx 2\int_{x(R1)}^{x(R2} k(x)dx.
\end{aligned} \tag{37}$$

Here $\hat{\beta}$ in both (34) and (37) is the phase shift that results from the roundtrip travel path between the two resonance locations $x(R1)$ and $x(R2)$. In Figure 5, (28) indicates that η should be significantly large ($\gg 1$) near the minimum resonance frequency since neither

f_1 nor f_2 is large and the gradient is also very small, which corresponds to $\xi \to 0$, $\zeta \to 1$. Then (36) is reduced to $A = 1$, which is consistent with the result in Figure 5. Since this η is sufficiently large, the absorption remains perfect until the frequency approaches f_{cH} or $f_1 \to \infty$. The minimum of A that is expected from (36) occurs when $\cos\hat{\beta} = 1$ is satisfied:

$$A_{min}(\zeta) = 1 - \frac{(1+\zeta^2)}{(1+\zeta)^2} \tag{38}$$

Since ζ is still relatively close to 1, we have $A_{min} \to 0.5$ where $\hat{\beta} = 2n\pi$ is satisfied. Thus, near f_{cH}, it is expected that harmonic structure arises with the absorption varying from 1 to about 0.5. This feature is consistent with the result of Figure 5 in the sense that such harmonic variation occurs when the frequency increases up to f_{cH}. Our analogy with a three-layered problem suggests that such harmonic variations (which in this case range from 0.5 to 1) are possible in the absorption coefficient because of the interference between the forward and backward waves that propagate between the two resonances.

3.4. Dependence on Electron and Heavy Ion Densities

The mode conversion efficiency discussed in Section 3.2 indicates that the absorption should strongly depend on frequency, ion density gradients as well as electron density. In this section, we examine the resonant absorption for different electron and heavy ion densities. In the step-like case of Figure 1a, Figure 7 shows how the resonant absorption occurs over different background electron densities from 0.5 to $1000cm^{-3}$. Here the gradient scale and $\lambda_{\|}$ are assumed to be $0.3R_E$ and $2.0R_E$, respectively, which cover the same range of values in Figure 2.

Figure 7a (7b) shows the absorption when the wave is incident from a H^+-rich (He^+-rich) to a He^+-rich (H^+-rich) plasma. Figure 7a indicates that the absorption becomes relatively effective when the total density decreases. When the density increases, the absorption becomes significant only near each cyclotron frequency of H^+ and He^+ ion, respectively. This feature is well understood if we consider the role of n_e in (28). In order to obtain large absorption, $|k_0 a|$ should reach such a small value as 0.22 and it prefers a relatively low n_e, which is consistent with the result in Figure 7a. When n_e increases, $|k_0 a|$ in (28) can be small only when either $f_1 \rightarrow \infty$ ($\omega \approx \omega_{cH}$) or $f_2 \rightarrow \infty$ ($\omega \approx \omega_{cHe}$) is satisfied. It is evident that the absorption in Figure 7a tends to be limited to each ion cyclotron frequency for relatively large n_e.

Figure 7b shows that the absorption variation becomes roughly opposite to that in Figure 7a. As discussed in detail in Section 3.2, if n_e increases and $|k_0 a|$ becomes sufficiently large in (28), the absorption becomes perfect in most frequencies in (31). When the density decrease in Figure 7b, it is evident that the absorption becomes gradually reduced from both ion cyclotron frequencies where $|k_0 a|$ is relatively small. However, as shown in Figures 3 and 7b, this type of absorption always remains important over the intermediate frequency range between the two cyclotron frequencies.

Figure 8 shows the absorption in the bump-like case of Figure 1b. Figure 8a (8b) shows the absorption when there is the density bump in n_{He} (n_H), respectively. The size of the inhomogeneous bump is assumed to be $0.6R_E$ and $\lambda_{\|} = 2.0R_E$ is used. The variation of $\delta n_j/n_e$ is from 0.001 at both edges to 0.3 at the top of the crest, which is the same as in Figure 4. In Figure 8a, the absorption occurs over a large frequency band when the density is small, but becomes restricted again to $\omega \approx \omega_{cHe}$ when the density increases.

This is consistent with condition (28) that small values of $|k_0 a|$ are required to have large absorption. Since the maximum composition of He^+ ions is 30% in this bump-like profile unlike 100% in the step-like case above, the resonance frequency cannot reach ω_{cH}. Since $f_1 \rightarrow \infty$ ($\omega \approx \omega_{cH}$) is impossible, there is no absorption elsewhere as discussed in Section 3.3. It is also confirmed that the absorption peak maximized around 0.25 and 0.5 for various background density values in Figures 7a and 8a, respectively, consistent with our estimate based on the Budden solution.

The harmonic structure caused by the interference between the forward and backward waves propagating between the two resonances has dependence on both the electron density in Figure 8b and the gradient scale in Figure 5. Between the two neighboring peaks, $\delta\hat{\beta} \approx 2\pi$ should be satisfied. If we assume that k_{eff} and $X_R = x(R1) - x(R2)$ are the effective wavenumber and distance between the two resonances, we can approximate $\hat{\beta}$ as $2k_{eff}X_R$, which is reduced to

$$\delta\hat{\beta} = 2(\delta k_{eff} X_R + k_{eff}\delta X_R) \approx 2\pi \tag{39}$$

Here k_{eff} and X_R should be proportional to k_0 and the total size of the bump, respectively. For instance, if the density profile of the H^+ bump is fixed by X_R, the harmonics would be determined simply by the wavenumbers and we obtain $\delta k_{eff} X_R \approx \pi$. From Appendix B, we have

$$k_0 = \sqrt{\frac{\Delta'}{\delta'}} \approx \sqrt{\frac{f_2 - 16f_1}{4f_1 - f_2} 2D_0 Y_{He}} \propto \sqrt{\frac{n_e}{\omega}}. \tag{40}$$

Thus, $\delta k_{eff} X_R \approx \pi$ and (40) give $\delta\omega \propto \omega^{3/2}/n_e^{1/2}$, which shows that $\delta\omega$ between the neighboring harmonics is inversely proportional to $n_e^{1/2}$. It is consistent with the feature in Figure 8b that $\delta\omega$ increases for relatively small n_e.

Up to now, we have assumed that the incident waves start from the region of either H^+ or He^+ dominant plasmas in both step-like and bump-like cases. It is interesting to examine the mode conversion process when the incident wave is from the region of H^+-He^+ mixture. In Figure 9, we assume such cases where N_{H+} is the background H^+ density in the region of incident waves. The H^+ density drops by δN across the step-like profile in Figure 9a, or has a dip of δN across the bump-like profile of He^+. In the previous cases in Figure 1, $N_{H+} = 1.0$ and $\delta N = 1$ were used in the step-like profile, and $N_{H+} = 1.0$ and $\delta N = 0.3$ were used in the bump-like profile.

Figure 10a shows how the absorption occurs in Figure 9a when N_{H+} ranges from 0.5 (50% H^+ and 50% He^+) to 1.0 (100% H^+) where $\delta N = 0.5$ is assumed. The gradient scale is assumed to be $0.3R_E$ for convenience. The cutoff frequency and the maximum and minimum resonance frequencies are given by f_{co}, f_{bb}^{max} and f_{bb}^{min}, respectively. The absorption becomes significant in Figure 10a only when N_{H+} is close to either 1 or 0.5, which indicates that relatively large absorption arises only if either side of the uniform regions, where the incident waves or transmitted waves propagate, is composed of almost purely H^+ or He^+ ions. For instance, the absorption becomes negligible (< 0.1) if $N_{H+} < 0.90$, and the peak occurs approximately only for $N_{H+} > 0.95$. The other absorption peak occurs when $N_{H+} \sim 0.5$ or $N_{H+} - \delta N \ll 1$ is satisfied. This indicates that the absorption becomes significant only when any region has relatively small amount of minority ions.

Figure 10b shows the absorption when n_H and n_{He} are switched. Thus the incident wave is from He^+-rich plasma and N_{H+} ranges from 0.5 (50% H^+ and 50% He^+) to 0 (100% He^+). It should be noted that complete absorption occurs even though the background plasma is almost an arbitrary mixture of H^+ and He^+ unlike Figure 10a.

There are exceptions near the H^+ dominant region near f_{cHe}, which is already confirmed in the previous sections. Therefore, it is expected that the resonant absorption is effective only if the incident wave propagates from the region of relatively large n_{He} to the region of relatively small n_{He}.

Figure 11a shows the absorption of Figure 9b when N_{H+} ranges from 0.3 (30% H^+ and 70% He^+) to 1.0 (100% H^+) where $\delta N = 0.3$ is assumed. In Figure 11a, the absorption becomes important (larger than 0.1) only for $N_{H+} > 0.9$, which is consistent with the feature in Figure 10a. The bump-like profile also prefers a small amount of minority ions in exciting a significant resonant absorption. Unlike Figure 10a, the absorption becomes negligible where the plasma is composed of purely He^+ ions or $N_{H+} \approx \delta N = 0.3$. This feature is understandable because its location corresponds to the top of the crest in the He^+ density profile where the density gradient vanishes and consequently $|k_0 a|$ is large (28).

Figure 11b shows the absorption in the bump-like profile when n_H and n_{He} are switched (in Figure 9b). The incident wave is from the He^+-rich plasma, but has a dip in the middle where N_{He+} drops by $\delta N = 0.3$. Thus N_{H+} ranges from 0 (100% He^+) to 0.7 (70% H^+ and 30% He^+). Complete absorption occurs except in the region where $|k_0 a|$ is small, where harmonic variations resulting from wave interference between the resonances can be seen. Both Figures 10b and 11b suggest that complete absorption occurs whether the density profile is bump-like or step-like. When a wave is incident from a region of relatively large n_{He} to the region of relatively small n_{He}, a significant absorption should always be expected.

We assumed relatively large variation of the ion population in our density model. It may be the case that it is not common to see such large variation over a radial distance of $0.5R_E$ except at the plasmapause, etc., even though the heavy ion population variation sometimes becomes significant near geostationary orbit [*e.g., Fraser et al.,* 2005]. However, it should be noted that the resonance frequency not only varies because of changes in the ion population but also because of variation in the magnetic field. Indeed, even if the relative ion population ratio is maintained to be constant, the magnetic field from $L = 6.6$ to $L = 6.1$ over the same distance of $0.5R_E$ should change more than 25%, which results in the similar variation of the resonance frequencies as shown in Figures 1 and 2. Thus the resonance frequency in the magnetosphere varies in almost the same manner as presented above suggesting that our results should be applicable to the magnetospheric phenomena.

4. Discussion

4.1. Electrostatic and Electromagnetic Property

Magnetic field observations of Pc1-2 waves suggest that the wave events are primarily electromagnetic in nature nature rather than electrostatic. For convenience, we can estimate the ratio of each electric and magnetic field component by assuming the dispersion relation in a homogeneous plasma, where (2) becomes

$$\begin{pmatrix} S - n_\parallel^2 & -iD & n_\parallel n_\perp \\ iD & S - n^2 & 0 \\ n_\parallel n_\perp & 0 & P - n_\perp^2 \end{pmatrix} \begin{pmatrix} E_x \\ E_y \\ E_z \end{pmatrix} = 0. \tag{41}$$

Here $P \simeq 1 - \omega_{pe}^2/\omega^2 \simeq -\omega_{pe}^2/\omega^2 \gg 1$ when ion waves ($\omega \sim \Omega_i$) are considered, and $P \leq 1$ when an electron wave such as the upper hybrid wave is considered. From (41), we have

$$\frac{E_y}{E_x} = \frac{iD}{n^2 - S}$$

$$\frac{E_z}{E_x} = \frac{n_\parallel n_\perp}{n_\perp^2 - P} \tag{42}$$

and the magnetic field components are determined by (1) such as $c\mathbf{B} = (-n_\parallel E_y, n_\parallel E_x - n_\perp E_z, n_\perp E_y)$ and then we have the ratio of B components from (42):

$$\begin{aligned} \frac{B_y}{B_x} &= \frac{n_\parallel E_x - n_\perp E_z}{-n_\parallel E_y} = \frac{1 - \frac{n_\perp^2}{n_\perp^2 - P}}{\frac{-iD}{n^2 - S}} \\ \frac{B_z}{B_x} &= \frac{n_\perp E_y}{-n_\parallel E_y} = -\frac{n_\perp}{n_\parallel}. \end{aligned} \tag{43}$$

When the inhomogeneity lies perpendicular to $\mathbf{B_o}$, the cold plasma assumption implies that $n_\perp$ increases to infinity near the resonance point. However, in reality, this value is limited by kinetic effects such as Landau damping or the finite gyro-radius effect and dissipation. To maintain the validity of the cold fluid approach, the ion and electron waves are restricted by the condition, $k_\perp \rho_{ci} < 1$ and $k_\perp \rho_{ce} < 1$, respectively, where ρ_{ci} or ρ_{ce} are the gyro-radius of ions and electrons. If the temperature is assumed to be about the order of $10eV$ for both background cold ions and electrons, we obtain $\rho_{ci} \sim 4km$ and $\rho_{ce} \sim 0.1km$, which provide $k_{\perp max}$ and $\lambda_{\perp min}$ and the mode conversion would be modified by kinetic effects beyond this limit. Thus $n_{\perp max}$ is also determined by $k_{\perp max} c/\omega < c/\omega\rho$ in each case.

Let us consider the behavior near a resonance after an impulse, In the case that we neglect kinetic limitations and assume $n_\perp \to \infty$ in (42) and (43), we obtain the growth of E_x and the damping of both E_y and E_z from (42), also the damping of B_x from E_y, and the damping of B_y because $B_y/B_x \to P/iD$ as well as the damping of B_z because $B_z \to (iD/cn_\parallel)E_z$. Thus only E_x grows, and all the other components are damped at the resonance, which corresponds to the feature of the cold upper hybrid waves in numerical experiments [e.g. *Kim et al.*, 2005b]. Although that simulation applies to a different

frequency range, the same approximations apply—namely, that P, which has the largest value of all the tensor elements S, D and P, becomes negligibly small compared to ${n_\perp}^2_{max}$. Near the geostationary equatorial region in our model, upper hybrid waves are expected to satisfy

$$\frac{{n_\perp}^2_{max}}{P} \approx \frac{\left(\frac{c}{\omega\rho_{ce}}\right)^2}{1-\frac{\omega_{pe}^2}{\omega^2}} \sim 2.6\times 10^4 \gg 1, \tag{44}$$

which validates our assumption above that $n_\perp$ is large enough to neglect all the other terms.

However, when ion waves are considered in the geostationary equatorial region, we have ${n_\perp}^2_{max}/P \approx (c/\omega_{pe}\rho_{ci})^2 \sim 0.17 \ll 1$, which is the opposite to the case of electron waves above. This difference significantly modifies the ratio of B_y in (43)

$$\frac{B_y}{B_x} \approx -\frac{n^2-S}{iD} = -\frac{E_x}{E_y}, \tag{45}$$

indicating that B_y grows in time just like E_x. In fact, the relative ratio of ${n_\perp}^2_{max}/P$ is important in determining whether the resonant response can be electrostatic or electromagnetic. This feature suggests that the radial electric field (E_x) and the azimuthal magnetic field (B_y) are likely to be excited at the heavy ion resonance, which is similar to the case of shear Alfven modes in MHD waves. Unlike the electron waves, the electromagnetic waves are expected to occur with relatively strong linear polarization as long as ${n_\perp}^2_{max}/P \ll 1$ is satisfied.

4.2. BuchsBaum-Bers Resonances *vs*. Ion-Ion Hybrid Resonances

It is useful to discuss the relative roles of the Buchsbaum-Bers (BB) resonance ($S=0$) and the ion-ion hybrid (II) resonance ($S=n_\parallel^2$). It should be noted that the BB resonance has no k-dependence, which means that there is no propagation in the cold plasma limit.

By definition, it should have an electrostatic nature in that the electric field parallel to the $\mathbf{k}_\perp$ grows, while the other components damp via the mode conversion. On the other hand, the II resonance has $k_\parallel$-dependence, which allows propagation along the magnetic field lines with electromagnetic nature just like shear Alfvén waves in MHD. Thus the two resonances can be distinguished in the cold plasma limit by the electrostatic (BB) or electromagnetic (II) nature, although the two resonance locations are close to each other when $n_\parallel$ (or $k_\parallel$) becomes relatively small.

When electron inertial effects are included in a cold, fluid model, there is a fourth order system of equations supporting two different modes (each forward and backward propagating) and the only resonance is the BB resonance and there is no resonance at $S = n_\parallel^2$. However, when electron inertial effects are ignored, only one of the modes (an ion mode) can be described with a resonance at the II resonance location and there is no resonance at $S = 0$. In order to understand the role of the II resonance, it is necessary to consider the fourth order equation. It should be noted that away from these resonances, there are two modes in the system with far different scales—a compressional ion Alfvén-like mode and a short scale electron inertial mode. If we go back to the full wave dispersion relation of (19) and (21), we find the two modes of large and small $n_\perp$, respectively:

$$n_\perp^2 \approx \begin{cases} \frac{(P+S)\delta - D^2}{S} - \frac{\delta^2 - D^2}{\delta} \\ \frac{\delta^2 - D^2}{\delta}, \end{cases} \tag{46}$$

where the second mode is the ion wave that was derived in (22). The first mode, where the first term is very large compared to the second term near the resonance, is an electron inertial wave which can be approximated as

$$n_\perp^2 \approx \frac{(P+S)\delta - D^2}{S} \approx \frac{P\delta}{S}. \tag{47}$$

It should be noted that when P is large, the electron inertial mode is heavily damped everywhere except between the BB and II resonances and therefore that mode is only important in a small region near the two resonances. (47) shows that the resonance of electron waves is determined by $S = 0$, where (47) becomes $n_\perp^2 \approx -Pn_\parallel^2/S$. This is equivalent to the original resonance condition of $\tan^2\theta = -P/S$ from (5), where the BB resonance is defined. Strictly speaking, the BB resonance ($S = 0$) implies a resonance of the electron inertial scale waves rather than that of ions in the sense that $n_\perp$ should be so large that the wavelength becomes too small to represent the wave motion of ions.

When we completely neglect the effect of electron inertia, the full wave equations are reduced to the second order differential equation of the ion waves, which is similar to the Budden problem near the resonance. Thus the II resonance takes energy from the fast wave at $S = n_\parallel^2$ and launches a resonant wave along the magnetic field lines. The second mode in (46) allows a sufficiently small $n_\perp$ or large wavelength for the ion motion when the leading term of (47) is removed. Since the dispersion relation $n_\perp^2 \approx (\delta^2 - D^2)/\delta$ has no dependence on P (associated with the electron inertia), it is evident that the resonance of $\delta = 0$ or $S = n_\parallel^2$ is composed of ion motion. Thus, the II resonance represents the resonance of ion waves.

A solution of the fourth order dispersion relation including the effect of electron inertia shows that near the II resonance location the two approximate solutions given above break down because the spatial scale of the modes becomes comparable. The ion and electron branches couple at the II resonance location giving rise to two complex conjugate solutions with wavelength comparable to the ion mode. No resonance occurs for either mode at the II resonance location. However, the modes are strongly coupled in that region ($S \approx n_\parallel^2$)

leading to mode conversion from the ion wave to the electron inertial wave. Some of the wave Poynting flux remains in a transmitted ion wave which propagates unaffected through the $S = 0$ resonance. On the other hand, the mode-converted electron inertial wave carries wave Poynting flux into the principal resonance $S = 0$ where it is absorbed in the cold plasma limit. We have found that this energy absorption is the same as the energy absorption that occurs at the II resonance when electron inertial effects are ignored provided that there is a principal resonance ($S = 0$) allowed by the profile, which suggests that the electron inertial wave carries all the mode converted wave energy to the principal resonance. On the other hand, if there is only an II resonance without a BB resonance for a given profile, the ion waves are mode-converted at the II resonance to electron inertial waves that propagate away from the II resonance region without any resonant absorption. This property of the solutions explains why the absorption only exists over the frequency range of $S = 0$ rather than $S = n_{\|}^2$ in Figures 2-5, even though the ion waves have a resonance at $S = n_{\|}^2$. It is expected that the electron inertial waves between the II resonance and the BB resonance are essentially dispersive waves associated with a resonance field-aligned mode $S = n_{\|}^2$. As the waves carry energy into the $S = 0$ resonance, it would be expected that they become electrostatic in nature.

In a realistic warm plasma, it is expected that the waves would not become fully electrostatic in nature for several reasons. First, there would be a kinetic limit for large $n_\perp$ and second, if field-aligned propagation is faster than dispersion across the magnetic field, the wave energy could be absorbed at some other location. If we examine the dispersion relation (47) of the electron wave (the waves including P-dependence), we can assume that $n_\perp$ is large, although it will be bounded because of kinetic physics. For in-

stance, $n_{\perp max}$ can be limited by the finite gyro-radius, which is estimated in Section 4.1 as $n_{\perp max}^2/P \approx (c/\omega_{pe}\rho_{ci})^2 \sim 0.17 \ll 1$ for $10eV$-ions near the geosynchronous orbit. Then we have a dispersion relation near the resonance from $n_\perp^2 \approx P\delta/S$ in (47):

$$S \approx \frac{n_\parallel^2}{1-\frac{n_\perp^2}{P}} \approx \frac{n_\parallel^2}{1+\frac{k_\perp^2 c}{\omega_{pe}^2}} \tag{48}$$

since $P \approx= -\omega_{pe}^2/\omega^2$. As $k_\perp$ becomes large, $S \to 0$ consistent with the resonance condition. When $k_\perp$ is so small that the wavelength becomes larger than the electron inertia length, we have $S = n_\parallel^2$, where it couples with the II resonance. This dispersion relation describes dispersive electron inertial waves that mode convert from fast waves at the II resonance and radiate energy away to the BB resonance location. This feature is similar to the nature of the inertial Alfven wave since $S \to c^2/V_A^2$ in the low frequency limit where V_A is the Alfven speed. Therefore, the relationship between the two resonances in the cold plasma limit can be understood. Since our results suggest that the ion-ion hybrid resonance $S = n_\parallel^2$ or (48) is likely to act as a real resonance for relatively small $n_\perp$ or $n_\perp^2/P$, the electromagnetic resonances II resonant waves are expected to propagate along the magnetic field lines with dispersion across the magnetic field due to electron inertial effects. This result is found to be consistent with the characteristics of statistical observations near the equatorial region [e.g. *Anderson et al.*, 1992b; *Fraser and Nguyen*, 2001].

4.3. Resonance Frequency and Heavy Ion Composition

When $\omega_{pe} \gg \omega_{ce}$ is satisfied, the resonance condition ($S = 0$) is determined only by the magnetic field intensity and the population ratios among the multiple ions. Figure 12 shows how two- and three-ion cases have resonance frequencies, which suggest that

from this resonance is is possible to infer the relative concentration of each ion in the background plasma. If two ions are involved, a measurement of the resonance frequency f_{bb} directly provides the composition ratio. If more ions are involved, we would find an additional branch satisfying $S = 0$ in Figure 12b. Each resonance would be located in between each band of ion cyclotron frequencies such as f_{b1} (He^+ branch) and f_{b2} (O^+ branch), respectively, in Figure 12b. The resonance frequency varies in a simple manner in that it increases (decreases) as its heavier ion composition increases (decreases). In Figure 12a, f_{bb} decreases as n_{He}/n_e decreases in x. In Figure 12b, it is clear that f_{b1} and f_{b2} tend to vary by the density variation of He^+ and O^+, respectively. This feature could be used to monitor the heavy ion population by investigating Pc1-2 wave events near the ion cyclotron frequencies. It should be noted that near the resonance the wave solutions would be linearly polarized, which correspond to E_x and B_y in our model above. Thus, when linearly polarized Pc1-2 events are found around each cyclotron frequency of ions in space, we could use the peak frequencies to determine the abundance of heavy ions near the location of the observation.

Our results showed that the resonant absorption should significantly depend on the direction of incident waves relative to the density gradient. If the fast wave propagates from the source region into the region where the resonance frequency profile (or the heavier ion population) increases, relatively small absorption occurs only when the minority ions are a few percent and the frequency should be close to each ion cyclotron frequency. If the fast wave propagates into the region where the resonance frequency (or the heavier ion population) decreases, it is strongly absorbed except for the case of a small relative density of minority ions. For instance, if the source is located at $x > X$ in Figure 12b,

only f_{b2} would have strong absorption since this branch is decreasing in the direction of the incident wave propagation. If the source is located at $x < 0$, f_{b2} would have strong absorption as long as the least population of minority ions are more than a few percent.

It is expected that several observational features of Pc1-2 waves could be explained by our results. For instance, *Anderson et al.* [1991] showed a puzzling case of Pc1-2 waves in the magnetosheath plasma consisting of He^+, He^{++}, O^+ where the polarization becomes left-handed above $f_{He^{++}}$ and linearly-polarized below $f_{He^{++}}$. Our results indicate that such a differential polarization pattern could happen if the He++ density decreases and O+ increases toward the wave source region. When the source frequency is broad-banded, the waves would be linearly-polarized below $f_{He^{++}}$ because of the strong resonant absorption, while the waves above $f_{He^{++}}$ would remain either left-handed or right-handed polarized.

Another consequence of this study for a realistic magnetospheric geometry can be inferred from the topology of the resonant frequency profiles. If one considers fixed plasma concentrations and magnetic field variation, the resonance frequency is proportional to the magnetic field so the resonance profile would be topologically similar to the case of Figure 2 for waves propagating inward (to smaller L) and Figure 3 for waves propagating outward (note waves are launched from the right). Therefore, it would expected that waves propagating outward would be absorbed most efficiently.

4.4. Effects of Warm Plasmas

In our model we assumed the cold plasma limit. In a high β plasma it would be important to also include kinetic effects. Mode conversion of fast Alfven waves at the ion-ion hybrid resonances has been extensively examined with models that include thermal

effects [e.g. *Swanson*, 1976; *Jacquinot et al.*, 1977; *Perkins*, 1977; *Lapierre*, 1983; *Brambilla and Ottaviani*, 1985; *Riyopoulos and Tajima*, 1986; *Lashmore-Davies et al.*, 1988; *Fuchs et al.*, 1995]. The mode conversion in warm plasmas indicates that the II resonance typically leads to the electron heating via the excitation of ion Bernstein waves [e.g. *Swanson*, 1976; *Brambilla and Ottaviani*, 1985; *Lashmore-Davies et al.*, 1988; *Majeski et al.*, 1994; *Fuchs et al.*, 1995]. As discussed in the previous sections 4.1 and 4.2 above, our fluid model is restricted to relatively large scale phenomena ($> \rho_{ci}$).

The small-scale response at the resonance requires a kinetic treatment. For instance, the finite gyro-motion and resonant motion of each ion species directly affects the motion of electrons near the singularities of ion resonances in the fluid equations. In addition, to approximate the effect of warm plasma, the wave equations can be modified by replacing (4) by the kinetic dielectric tensor including the correction term of finite gyro-radius as the first-order approximation [*Swanson*, 1976]. These subjects are left as future work. Since the region in our model lies in a relatively cold regime ($\beta \sim 0.01$), it is expected that our results can be applied to most wave events in observations, although the exact nature of the resonant absorption needs to be clarified by a kinetic approach.

5. Conclusion

In order to focus on basic properties of the wave coupling at the heavy ion resonances, we have considered the cases of two ions for simplicity in this study. When more ions such as O^+ are involved, there are more branches of resonances as indicated in Figure 12b. The resonant absorption would become rather complicated in the sense that the gradient of each resonance frequency can be positive and negative at the same time and there are many cases in the choices of minority ions. However, our result suggest that the

absorption can be reduced to that of Budden problem near each resonance once the heavy ion density profiles are given, which would enable us to understand the effect of more ion cases.

We have also assumed that the background magnetic field is constant and the total density of ions or electrons is constant in order to focus on the role of heavy ion composition. In fact, the condition of the resonant absorption (28) would depend on both the gradient of magnetic field and electron density to some extent. It remains as a future work to study such additional effects of more ions, ∇B as well as ∇n_e.

The presence of heavy ions invokes a new resonance, which is composed of the hybrid ion motions. Unlike the electron wave resonance, this heavy ion resonance is found to have strong electromagnetic nature. These resonances are expected to occur with the linear polarization near the multi-ion hybrid resonances, which could be important in determining the heavy ion composition in space.

Appendix A: Derivation of the Coupled Wave Equations in Multi-Ion Plasmas

The coupled equations of (8) are written in terms of E_y and cB_y, which represent the eigenstates in vacuum. If the uniform plasmas are introduced at both sides of $x > X$ (Region 1) and $x < 0$ (Region 2), and the nonuniform region lies within $0 \leq x \leq X$, we can change (8) into the wave equations in terms of the eigenstates of plasma waves as follows:

$$\frac{d^2\phi}{dx^2} - \frac{d\tilde{\mathcal{E}}(x)}{dx}\tilde{\mathcal{E}}^{-1}(x)\frac{d\phi}{dx} + \tilde{\mathcal{E}}(x)H^2\tilde{\mathcal{M}}(x)\phi = 0 \tag{A1}$$

where

$$\phi \;=\; C_1^{-1}\psi = C_1^{-1}\begin{pmatrix} E_y \\ cB_y \end{pmatrix},$$

$$\begin{aligned}
\tilde{\mathcal{E}}(x) &= C_1^{-1}\mathcal{E}(x)C_1, \\
\tilde{\mathcal{M}}(x) &= D_1^{-1}C_1^{-1}\mathcal{M}(x)C_1, \\
D_1 &= C_1^{-1}\mathcal{M}_1 C_1, \\
H^2 &= \frac{\omega^2}{c^2}D_1 = \begin{pmatrix} h_1^2 & 0 \\ 0 & h_2^2 \end{pmatrix}.
\end{aligned} \tag{A2}$$

Here C_1 is the linear transformation matrix from the plasma wave eigenstates of Region 1 to the vacuum TE and TM modes. D_1 and H are the diagonal matrix, where h_j represents the x component wavenumber of the j-th eigenstate in Region 1. Thus (A1) and (11) show that both $\tilde{\mathcal{E}}_1$ and $\tilde{\mathcal{M}}_1$ become the unit matrix in Region 1. The boundary conditions for $\phi(x)$ in (A1) are given by

$$\begin{aligned}
\phi(x)|_{x-\epsilon} &= \phi(x)|_{x+\epsilon} \\
\frac{1}{\tilde{\mathcal{E}}(x)}\frac{d\phi}{dx}|_{x-\epsilon} &= \frac{1}{\tilde{\mathcal{E}}(x)}\frac{d\phi}{dx}|_{x+\epsilon}\ .
\end{aligned} \tag{A3}$$

In order to decompose the wave function in terms of the coupling components, we can extend (A1) as

$$\frac{d^2\Phi}{dx^2} - \frac{d\tilde{\mathcal{E}}(x)}{dx}\tilde{\mathcal{E}}^{-1}(x)\frac{d\Phi}{dx} + \tilde{\mathcal{E}}(x)H^2\tilde{\mathcal{M}}(x)\Phi = 0 \tag{A4}$$

where

$$\Phi(x) = \begin{pmatrix} \Phi_{11} & \Phi_{12} \\ \Phi_{21} & \Phi_{22} \end{pmatrix}. \tag{A5}$$

Here, Φij is the i-th component when the j-th component is an incident wave. In Region 1, the wave equation (A4) is simplified as follows:

$$\frac{d^2\Phi_1}{dx^2} + \tilde{\mathcal{E}}_1 H^2 \tilde{\mathcal{M}}_1 \Phi_1 = \frac{d^2\Phi_1}{dx^2} + H^2\Phi_1 = 0 \tag{A6}$$

where $\tilde{\mathcal{E}}_1$ and $\tilde{\mathcal{M}}_1$ are the unit matrix. When the incident wave is given by plane waves in Region 1, there are reflected waves in the same region and transmitted waves in Region

2. If the incident waves have a unit amplitude and the reflected waves are determined by the reflection coefficient matrix r in Region 1, we have

$$\Phi_1(x) = e^{-iH(x-X)} + e^{iH(x-X)} r(X) \tag{A7}$$

where

$$\begin{aligned} e^{-iH(x-X)} &= \begin{pmatrix} e^{-ih_1(x-X)} & 0 \\ 0 & e^{-ih_2(x-X)} \end{pmatrix}, \\ r(X) &= \begin{pmatrix} r_{11} & r_{12} \\ r_{21} & r_{22} \end{pmatrix}. \end{aligned} \tag{A8}$$

Here, $r_{ij}(X)$ is the reflection coefficient of the i-th component when the j-th component is an incident wave.

In Region 2 ($x < 0$) which is the uniform region of $\tilde{\mathcal{E}}_2$ and $\tilde{\mathcal{M}}_2$, (A4) becomes

$$\frac{d^2\Phi_2}{dx^2} + \tilde{\mathcal{E}}_2 H^2 \tilde{\mathcal{M}}_2 \Phi_2 = \frac{d^2\Phi_2}{dx^2} + M^2\Phi_2 = 0. \tag{A9}$$

However, $M^2 = \tilde{\mathcal{E}}_2 H^2 \tilde{\mathcal{M}}_2$ is no longer diagonal, and we can transform (A9) into

$$\frac{d^2\tilde{\Phi}_2}{dx^2} + Q^2\tilde{\Phi}_2 = 0 \tag{A10}$$

where

$$\begin{aligned} &\tilde{\Phi}_2 = C_2^{-1}\Phi_2, \\ &Q^2 = C_2^{-1} M^2 C_2 = \begin{pmatrix} q_1^2 & 0 \\ 0 & q_2^2 \end{pmatrix}. \end{aligned} \tag{A11}$$

Q is the diagonal matrix, and q_j represents the x component wavenumber of the j-th eigenstate in Region 2. Here C_2 is the linear transformation matrix from the plasma wave eigenstates of Region 2 to the eigenstates of Region 1. Thus, we can write the transmitted wave in Region 2 as

$$\tilde{\Phi}_2(x) = e^{-iQx} t(X) \tag{A12}$$

where $t_{ij}(X)$ represents the transmission coefficient of the i-th component when j-th component is an incident wave.

If we remove the inhomogeneous region ($X \to 0$), (A3) becomes the boundary conditions at $x = 0$ between the two uniform regions:

$$\begin{aligned}
&\Phi_1|_{x=0} = \Phi_2|_{x=0} = C_2\tilde{\Phi}_2|_{x=0} \\
&\frac{1}{\tilde{\mathcal{E}}_1}\frac{d\Phi_1}{dx}|_{x=0} = \frac{1}{\tilde{\mathcal{E}}_2}\frac{d\Phi_1}{dx}|_{x=0} = \frac{1}{\tilde{\mathcal{E}}_2}C_2\frac{d\tilde{\Phi}_2}{dx}|_{x=0}.
\end{aligned} \tag{A13}$$

From (A7) and (A12), (A13) becomes

$$\begin{aligned}
&I + r(0) = C_2 t(0) \\
&\frac{1}{\tilde{\mathcal{E}}_1} H\left(I - r(0)\right) = \frac{1}{\tilde{\mathcal{E}}_2} C_2 Q t(0).
\end{aligned} \tag{A14}$$

Since both $\tilde{\mathcal{E}}_1$ and $C_2^{-1}\tilde{\mathcal{E}}_2^{-1}C_2$ are the unit matrix I, $r(0)$ and $t(0)$ become

$$\begin{aligned}
&r(0) = C_2 t(0) - I \\
&t(0) = 2\Big(C_2 + H^{-1}C_2 Q\Big)^{-1}.
\end{aligned} \tag{A15}$$

Both (A6) and (A9) satisfy the conservation of $J = d\Phi^\dagger/dx\Phi - \Phi^\dagger d\Phi/dx$,

$$\begin{aligned}
J &= \frac{d\Phi_1^\dagger}{dx}\Phi_1 - \Phi_1^\dagger\frac{d\Phi_1}{dx} \\
&= \frac{d\Phi_2^\dagger}{dx}\Phi_2 - \Phi_2^\dagger\frac{d\Phi_2}{dx} \\
&= \frac{d\tilde{\Phi}_2^\dagger}{dx}\tilde{\Phi}_2 - \tilde{\Phi}_2^\dagger\frac{d\Phi_2}{dx}
\end{aligned} \tag{A16}$$

which should be conserved if the inhomogeneous region is neglected and there is no absorption through mode conversion. By putting (A7) and (A12) into (A16), we have the following condition:

$$H = r(0)^\dagger H r(0) + t(0)^\dagger Q t(0). \tag{A17}$$

For instance, if the incident wave is assumed to be the first kind (e^{-ih_1x}) in Region 1,

$$1 = |r_{11}|^2 + \frac{h_2}{h_1}|r_{21}|^2 + \frac{q_1}{h_1}|t_{11}|^2 + \frac{q_2}{h_1}|t_{21}|^2. \tag{A18}$$

Thus, when the mode conversion occurs in an inhomogeneous region, the absorption of mode conversion can be defined by

$$A_1 = 1 - \left(|r_{11}|^2 + \frac{h_2}{h_1}|r_{21}|^2 + \frac{q_1}{h_1}|t_{11}|^2 + \frac{q_2}{h_1}|t_{21}|^2\right). \tag{A19}$$

When the two uniform regions are identical ($C_2 = I$), the conditions become simplified as follows:

$$\begin{aligned}
\tilde{\mathcal{E}}_1 &= \tilde{\mathcal{E}}_2, \quad \tilde{\mathcal{M}}_1 = \tilde{\mathcal{M}}_2, \\
\Phi &= \tilde{\Phi}, \\
r(0) &= 0, \quad t(0) = I, \\
A_j &= 1 - (|r_{1j}|^2 + |r_{2j}|^2 + |t_{1j}|^2 + |t_{2j}|^2).
\end{aligned} \tag{A20}$$

Appendix B: Application of Heavy Ion Resonances to Budden Problem

In order to make an analogy with the Budden problem, we adopt the expressions for k_0 and a in an inhomogeneous plasma, which are derived in Section 3.2:

$$\begin{aligned}
k_0^2 &= \frac{\Delta'}{\delta'} \\
a &= -\frac{\Delta}{\Delta'} \\
|k_0 a| &= \left|\frac{\Delta}{\sqrt{\delta'\Delta'}}\right|
\end{aligned} \tag{B1}$$

where Δ and δ are defined in Section 3.2. Here the resonance is defined by $S = 0$ or $\delta \approx 0$ and the cutoff is defined by $\delta = D$ (or $\Delta = 0$), respectively. To approximate the solutions

near the resonance and cutoff, we assume the linear profiles such as

$$\begin{aligned} \delta &\approx \kappa x \\ \delta - D &\approx \tilde{\kappa}(x-a). \end{aligned} \tag{B2}$$

Near the resonance, the condition of $|\delta_0| \ll |\Delta_0|$ can be applied:

$$\begin{aligned} \Delta_0 &= \delta_0^2 - D_0^2 \approx -D_0^2 \\ \Delta_0' &= 2(\delta_0\delta_0' - D_0 D_0') \\ &\approx 2(\delta_0 - D_0)\kappa + 2D_0\tilde{\kappa} \\ &\approx 2D_0(\tilde{\kappa} - \kappa) \\ &= -2D_0 D', \end{aligned} \tag{B3}$$

which are consistent with our various profiles assumed above in this study.

From (4), S and D are given by

$$\begin{aligned} S &= 1 - \frac{X_H}{1-Y_H^2} - \frac{X_{He}}{1-Y_{He}^2} - \frac{X_e}{1-Y_e^2} \\ D &= \frac{X_H Y_H}{1-Y_H^2} + \frac{X_{He}Y_{He}}{1-Y_{He}^2} - \frac{X_e Y_e}{1-Y_e^2}. \end{aligned} \tag{B4}$$

where $X_j = \omega_{pj}^2/\omega^2$ and $Y_j = \omega_{cj}/\omega$. Since $X_j' = n_j' e^2/m_j\epsilon_o\omega^2$ and $n_H' = -n_{He}'$ when the total electron density remains constant, $X_H' = -4X_{He}'$ is satisfied:

$$\begin{aligned} \delta' &= X_{He}'(4f_1 - f_2) \approx \kappa \\ D' &= X_{He}' Y_{He}(f_2 - 16 f_1) \approx \kappa - \tilde{\kappa} \\ f_1 &= \frac{1}{1-Y_H^2} \\ f_2 &= \frac{1}{1-Y_{He}^2}. \end{aligned} \tag{B5}$$

From (B3)-(B5), $k_0 a$ in (B1) becomes

$$|k_0 a| \approx \frac{1}{\sqrt{2Y_{He}}X_{He}'} \left| \frac{D_0^{3/2}}{\sqrt{(4f_1 - f_2)(f_2 - 16f_1)}} \right|$$

$$\propto \omega^{5/2} \mid \frac{1}{n'_{He}} \frac{n_e^{3/2}}{\sqrt{(4f_1 - f_2)(f_2 - 16f_1)}} \mid . \quad \text{(B6)}$$

Acknowledgments. This work was supported by the Korea Research Foundation Grant funded by the Korean Government(KRF-2005-070-C00059). K.K. has been supported by the Korea Science and Engineering Foundation grant (No. R0A-2007-000-20113-0) funded by the Korean Government. Work at PPPL was supported by NASA grants(NNH04AB23I, NNH04AA73I, NNH04AA16I, NNG07EK69I, NNH07AF37I), NSF grant(ATM 0411392), and DOE Contract No. DE-AC02-76CH03073.

References

Anderson, B. J., S. A. Fuselier (1993), Magnetic pulsations from 0.1 to 4.0 Hz and associated plasma properties in the earth's subsolar magnetosheath and plasma depletion layer, *J. Geophys. Res., 98*, 1461-1479.

Anderson, B. J., S. A. Fuselier, and D. Murr (1991), Electromagnetic ion cyclotron waves observed in the plasma depletion layer, *Geophys. Res. Lett., 18*, 1955-1958.

Anderson, B. J., R. E. Erlandson, and L. J. Zanetti (1992a), A statistical study of Pc 1-2 magnetic pulsations in the equatorial magnetosphere 1. Equatorial occurrence distributions, *J. Geophys. Res., 97*, 3075-3101.

Anderson, B. J., R. E. Erlandson, and L. J. Zanetti (1992b), A statistical study of Pc 1-2 magnetic pulsations in the equatorial magnetosphere 2. Wave properties, *J. Geophys. Res., 97*, 3089-3101.

Anderson, B. J., R. E. Denton, G. Ho, D. C. Hamilton, S. A. Fuselier, and R. J. Strangeway (1996), Observational test of local proton cyclotron instability in the Earth's magnetosphere, *J. Geophys. Res., 101*, 21,527-21,544.

Andre, M. (1985), Dispersion surfaces, *J. Plasma Phys.*, *33*, 1-19.

Arnoldy, R. L., L. J. Cahill, Jr., M. J. Engebretson, L. J. Lanzerotti, and A. Wolfe (1988), Review of hydromagnetic wave studies in the Antarctic, *Rev. Geophys., 26*, 181-207.

Bagenal, F., T. E. Dowling, and W. B. McKinnon (2004), Jupiter, in *Jupiter* edited by F. Bagenal and T. E. Dowling and W. B. McKinnon, Cambridge University Press, Cambridge.

Bellman, R., and G. M. Wing (1992), *An Introduction to Invariant Imbedding*, John Wiley, New York.

Bossen, M., R. L. McPherron, and C. T. Russell (1976), Simultaneous Pc 1 observations by the synchronous satellite ATS-1 and ground stations - Implications concerning IPDP generation mechanisms, *J. Atmos. Terr. Phys., 38*, 1157-1167.

Budden, K. G. (1985), *The propagation of radio waves : the theory of radio waves of low power in the ionosphere and magnetosphere*, Cambridge Univ. Press, New York.

Brambilla, M., and M. Ottaviani (1985), Mode conversion near ion-ion hybrid and IC harmonic resonances in Tokamaks , *Plasma Phys. Controlled Fusion*, *27*, 1-17.

Buchsbaum, S. J. (1960), Resonance in a Plasma with Two Ion Species, *Phys. Fluids*, *3*, 418-420.

Chandrasekhar, S. (1960), *Radiative transfer*, Dover, New York.

Dowden, R. L. (1966), Micropulsation "nose whistlers". A helium explanation, *Planet. Space Sci.*, *14*, 1273.

Engebretson, M. J., W. K. Peterson, J. L. Posch, M. R. Klatt, B. J. Anderson, C. T. Russell, H. J. Singer, R. L. Arnoldy, and H. Fukunishi (2002), Observations of two types of Pc 1-2 pulsations in the outer dayside magnetosphere, *J. Geophys. Res., 107*,

1451, doi:10.1029/2001JA000198.

Fraser, B. J. (1972), Propagation of Pc1 micropulsations in a proton-helium magnetosphere, *Planet. Space Sci.*, *20*, 1883.

Fraser, B. J. (1985), Observations of ion cyclotron waves near synchronous orbit and on the ground, *Space Sci. Rev.*, *42*, 357-374.

Fraser, B. J., and R. L. McPherron (1982), Pc 1-2 magnetic pulsation spectra and heavy ion effects at synchronous orbit - ATS 6 results, *J. Geophys. Res., 87*, 4560-4566.

Fraser, B. J., and T. S. Nguyen (2001), Is the plasmapause a preferred source region of electromagnetic ion cyclotron waves in the magnetosphere?, *J. Atmos. Terr. Phys., 63*, 1225-1247.

Fraser, B. J., W. J. Kemp, and D. J. Webster (1989), Ground-satellite study of a Pc 1 ion cyclotron wave event, *J. Geophys. Res., 94*, 11,855-11,863.

Fuchs, V., A. K. Ram, S. D. Schultz, A. Bers, and C. N. Lashmore-Davies (1995), Mode conversion and electron damping of the fast Alfvén wave in a tokamak at the ion-ion hybrid frequency, *Phys. Plasmas*, *2*, 1637-1647.

Gendrin, R., S. Perraut, H. Fargetton, F. Glangeaud, and J.-L. Lacoume (1978), ULF waves - Conjugated ground-satellite relationships, *Space Sci. Rev.*, *22*, 433-442.

Gendrin, R., M. Ashour-Abdalla, Y. Omura, and K. Quest (1984), Linear analysis of ion cyclotron interaction in a multicomponent plasma, *J. Geophys. Res., 89*, 9119-9124.

Glassmeier, K.-H., F. M.Neubauer, N. F. Ness, and M. H. Acuna (1989), Standing hydromagnetic waves in the Io plasma torus - Voyager 1 observations, *J. Geophys. Res., 94*, 15,063-15,076.

Glassmeier, K.-H., P. N. Mager, and D. Y. Klimushkin (2003), Concerning ULF

pulsations in Mercurys magnetosphere, *Geophys. Res. Lett., 30*(18), 1928, doi: 10.1029/2003GL017175.

Glassmeier, K.-H., D. Klimushkin, C. Othmer, and P. Mager (2004), ULF waves at Mercury: Earth, the giants, and their little brother compared, *Adv. Space Res.*, *33*, 1875-1883, doi:10.1016/j.asr.2003.04.047.

Horne, R. B., and R. M. Thorne (1997), Wave heating of He+ by electromagnetic ion cyclotron waves in the magnetosphere: Heating near the H-He bi-ion resonance frequency, *J. Geophys. Res., 102*, 11,457-11,472, doi:10.1029/97JA00749.

Inhester, B., U. Wedeken, A. Korth, S. Perraut, and M. Stokholm (1984), Ground-satellite coordinated study of the April 5, 1979 events - Observation of O(+) cyclotron waves, *J. Geophys. Z. Geophys.*, *55*, 134-141.

Jacquinot, J., B. D. McVey, and J. E. Scharer (1977), Mode conversion of the fast magnetosonic wave in a deuterium-hydrogen Tokamak plasma, *Phys. Rev. Lett., 39*, 88-91, doi:10.1103/PhysRevLett.39.88.

Johnson, J. R., and C. Z. Cheng (1999), Can ion cyclotron waves propagate to the ground?, *Geophys. Res. Lett., 26*, 671-674, doi:10.1029/1999GL900074.

Johnson, J. R., T. Chang, and G. B. Crew (1995), A study of mode conversion in an oxygen-hydrogen plasma, *Phys. Plasmas*, *2*, 1274-1284.

Kim, E.-H., J. R. Johnson, and D.-H. Lee (2008), Field line resonance at Mercury's magnetosphere: A simulation study, submitted to *J. Geophys. Res.*

Kim, K., and D.-H. Lee (2005), Invariant imbedding theory of mode conversion in inhomogeneous plasmas. I. Exact calculation of the mode conversion coefficient in cold, unmagnetized plasmas, *Phys. Plasmas*, *12*, 2101, doi:10.1063/1.1914536.

Kim, K., and D.-H. Lee (2006), Invariant imbedding theory of mode conversion in inhomogeneous plasmas. II. Mode conversion in cold, magnetized plasmas with perpendicular inhomogeneity, *Phys. Plasmas*, *13*, 2103, doi:10.1063/1.2186529.

Kim, K., D.-H. Lee, and H. Lim (2005), Theory of the propagation of coupled waves in arbitrarily inhomogeneous stratified media, *Europhys. Lett.*, *69*, 207-213, doi: 10.1209/epl/i2004-10341-0.

Kim, K.-S., E.-H. Kim, D.-H. Lee, and K. Kim (2005b), Conversion of ordinary and extraordinary waves into upper hybrid waves in inhomogeneous plasmas, *Phys. Plasmas*, *12*, 2903, doi:10.1063/1.1896285.

Klyatskin, V. I. (1994), The imbedding method in statistical boundary-value wave problems, *Prog. Opt.*, *XXXIII*, 1.

Klyatskin, V. I., N. V. Gryanik, and D. Gurarie (1998), Propagation and localization of Rossby waves over random topography (two-layer model), *Wave Motion*, *28*, 333.

Kozyra, J. U., T. E. Cravens, A. F. Nagy, E. G. Fontheim, and R. S. B. Ong (1984), Effects of energetic heavy ions on electromagnetic ion cyclotron wave generation in the plasmapause region, *J. Geophys. Res., 89*, 2217-2233.

Lapierre, Y. (1983), Magnetosonic wave propagation in the mode conversion regime, *J. Plasma Phys.*, *29*, 223-241.

Lashmore-Davies, C. N., V. Fuchs, G. Francis, A. K. Ram, A. Bers, and L. Gauthier (1988), A theory of fast-wave absorption, transmission, and reflection in the ion cyclotron range of frequencies, *Phys. Fluids*, *31*, 1614-1622.

Lee, D.-H., M. K. Hudson, K. Kim, R. L. Lysak, and Y. Song (2002), Compressional MHD wave transport in the magnetosphere 1. Reflection and transmission across the

plasmapause, *J. Geophys. Res., 107*, 1307, doi:10.1029/2002JA009239.

Lee, D.-H., K. Kim, E.-H. Kim, and K.-S. Kim (2006), Theoretical Studies of Plasma Wave Coupling: A New Approach, in *Geospace Electromagnetic Waves and Radiation, Lec. Notes Phys., Berlin Springer Verlag*, vol. 687, edited by J. W. Labelle and R. A. Treumann, pp. 235.

Majeski, R., C. K. Phillips, and J. R. Wilson (1994), Electron heating and current drive by mode converted slow waves, *Phys. Rev. Lett., 73*, 2204-2207, doi: 10.1103/PhysRevLett.73.2204.

Mauk, B. H., and R. L. McPherron (1980), An experimental test of the electromagnetic ion cyclotron instability within the earth's magnetosphere, *Phys. Fluids*, *23*, 2111-2127.

Mauk, B. H., C. E. McIlwain, and R. L. McPherron (1981), Helium cyclotron resonance within the earth's magnetosphere, *Geophys. Res. Lett., 8*, 103-106.

Ngan, Y. C., and D. G. Swanson (1977), Mode conversion and tunneling in an inhomogeneous plasma, *Phys. Fluids*, *20*, 1920-1937.

Perkins, F. W. (1977), Heating Tokamaks via the ion-cyclotron and ion-ion hybrid resonances, *Nucl. Fusion*, *17*, 1197-1224.

Perraut, S., R. Gendrin, A. Roux, and C. de Villedary (1984), Ion cyclotron waves - Direct comparison between ground-based measurements and observations in the source region, *J. Geophys. Res., 89*, 195-202.

Ram, A. K., A. Bers, S. D. Schultz, and V. Fuchs (1996), Mode conversion of fast Alfvén waves at the ion-ion hybrid resonance, *Phys. Plasmas*, *3*, 1976-1982.

Rammal, R., and B. Doucot (1987), Invariant imbedding approach to localization, I, General framework and basic equations, *J. Phys.*, *48*, 509.

Rauch, J. L., and A. Roux (1982), Ray tracing of ULF waves in a multicomponent magnetospheric plasma - Consequences for the generation mechanism of ion cyclotron waves, *J. Geophys. Res., 87*, 8191-8198.

Riyopoulos, S., and T. Tajima (1986), Simulation study of two-ion hybrid resonance heating, *Phys. Fluids*, *29*, 4161-4173.

Roux, A., S. Perraut, J. L. Rauch, C. de Villedary, G. Kremser, A. Korth, and D. T. Young (1982), Wave-particle interactions near Ω_{He^+} observed on board GEOS 1 and 2. II - Generation of ion cyclotron waves and heating of He^+ ions, *J. Geophys. Res., 87*, 8174-8190.

Smith, R. L., and N. Brice (1964), Propagation in Multicomponent Plasmas, *J. Geophys. Res., 69*, 5029.

Summers, D., and R. M. Thorne (2003), Relativistic electron pitch-angle scattering by electromagnetic ion cyclotron waves during geomagnetic storms, *J. Geophys. Res., 108*(A4), 1143, doi:10.1029/2002JA009489.

Swanson, D. G. (1976), Mode conversion and tunneling at the two-ion hybrid resonance, *Phys. Rev. Lett., 36*, 316-319.

Swanson, D. G. (1985), Radio frequency heating in the ion-cyclotron range of frequencies, *Phys. Fluids*, *28*, 2645-2677.

Young, D. T., S. Perraut, A. Roux, C. de Villedary, R. Gendrin, A. Korth, G. Kremser, and D. Jones (1981), Wave-particle interactions near ω_{He+} observed on GEOS 1 and 2. I - Propagation of ion cyclotron waves in He^+-rich plasma, *J. Geophys. Res., 86*, 6755-6772.

Figure 1. The density models of H^+ and He^+. The total density is constant as $n_e = n_H + n_{He} = 10/cm^3$. The ion density profiles are given by n_H (dotted line) and n_{He} (dashed line): (a) the three different gradient scales marked by (1, 2, 3) are assumed to be $\Lambda = 0.2, 0.5,$ and $1.0R_E$, respectively, in the step-like cases, and (b) three different bump sizes marked by (1, 2, 3) are assumed to be $0.4, 1.0,$ and $2.0R_E$ in the bump-like cases.

Figure 2. The left column shows the frequency profiles of Buchsbaum-Bers and ion-ion hybrid resonances in the step-like profile shown in Figure 1a for different field-aligned wavelength, $\lambda_\parallel$, when $n_e = 10/cm^3$ is assumed. The horizontal axis is normalized by Λ, which represents each gradient scale in the step-like profiles. The right column is the resonant absorption for each case. The line segment labeled f_{bb} is the range of possible resonance frequency shown in the left column. The different scales of $\Lambda = 0.2, 0.5,$ and $1.0R_E$ in Figure 1a are marked by 1, 2 and 3, respectively.

Figure 3. The same profiles as in Figure 2 when n_H and n_{He} are switched in Figure 1a.

Figure 4. The left column shows f_{bb} and f_{ii} in a bump-like profile in Figure 1b for different $\lambda_\parallel$ when $n_e = 10/cm^3$ is assumed. The different bump sizes of 0.4, 1.0, and 2.0 R_E in Figure 1b are marked by 1, 2 and 3, respectively.

Figure 5. The same profiles as in Figure 4 when n_H and n_{He} are switched in Figure 1b.

Figure 6. The radial wavenumber variation and the coefficients of reflection and transmission in the Budden problem when the incident wave propagates from a H^+-rich to a He^+-rich plasma region: (a) a single resonance in a monotonic step-like profile in Figure 1a, and (b) two resonances in a bump-like profile in Figure 1b.

Figure 7. The resonant absorption in a step-like profile of Figure 1a for different n_e: (a) when the incident wave propagates from a H^+-rich to a He^+-rich plasma, and (b) when the incident wave propagates from a He^+-rich to a H^+-rich plasma where $n_H \leftrightarrow n_{He}$.

Figure 8. The resonant absorption in a bump-like profile of Figure 1b for different n_e: (a) when the incident wave propagates from a H^+-rich to a He^+-rich plasma, and (b) when the incident wave propagates from a He^+-rich to a H^+-rich plasma where $n_H \leftrightarrow n_{He}$.

Figure 9. The (a) step-like and (b) bump-like density models where N_{H+} and δN are the residual H^+ density and its variation in the region of incidence, respectively. The total ion density is kept constant.

Figure 10. The absorption for profiles shown in Figure 9a for different N_{H+}. The gradient scale is assumed to be $0.3R_E$ and $\delta N = 0.5$ is assumed. The cutoff frequency and the maximum and minimum resonance frequencies are given by f_{co}, f_{bb}^{max} and f_{bb}^{min}, respectively: (a) when the incident wave propagates from a H^+-rich to a He^+-rich plasma, and (b) when the incident wave propagates from a He^+-rich to a H^+-rich plasma where $N_{H+} \leftrightarrow N_{He+}$ in the profile shown in Figure 9a.

Figure 11. The absorption for profiles shown in Figure 9b for different N_{H+}. The bump size is assumed to be $0.6R_E$ and $\delta N = 0.3$ is assumed. (a) when the incident wave propagates from a H^+-rich to a He^+-rich plasma, and (b) when the incident wave propagates from a He^+-rich to a H^+-rich plasma where $N_{H+} \leftrightarrow N_{He+}$ in the profile shown in Figure 9b.

Figure 12. The density models and the resonance frequency profiles for: (a) two ions and (b) three ions. In the three-ion case of (b), f_{b1} and f_{b2} are the resonances of the $H^+ - He^+$ branch and the $He^+ - O^+$ branch, respectively.

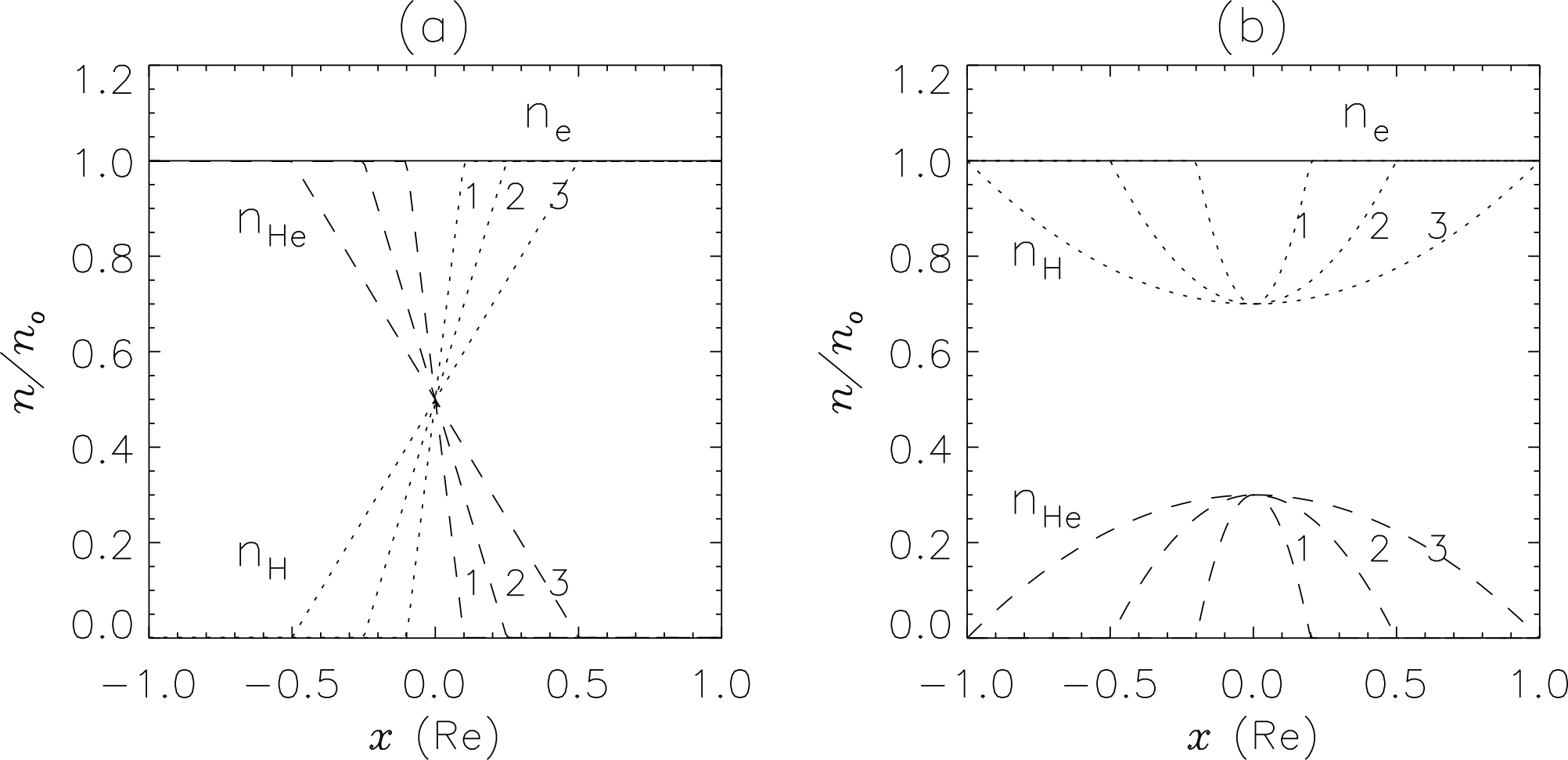
(a)
(b)
n_e
n_{He}
n_H
1
2
3
n/n_o
x (Re)
1.2
1.0
0.8
0.6
0.4
0.2
0.0
−1.0
−0.5
0.0
0.5
1.0

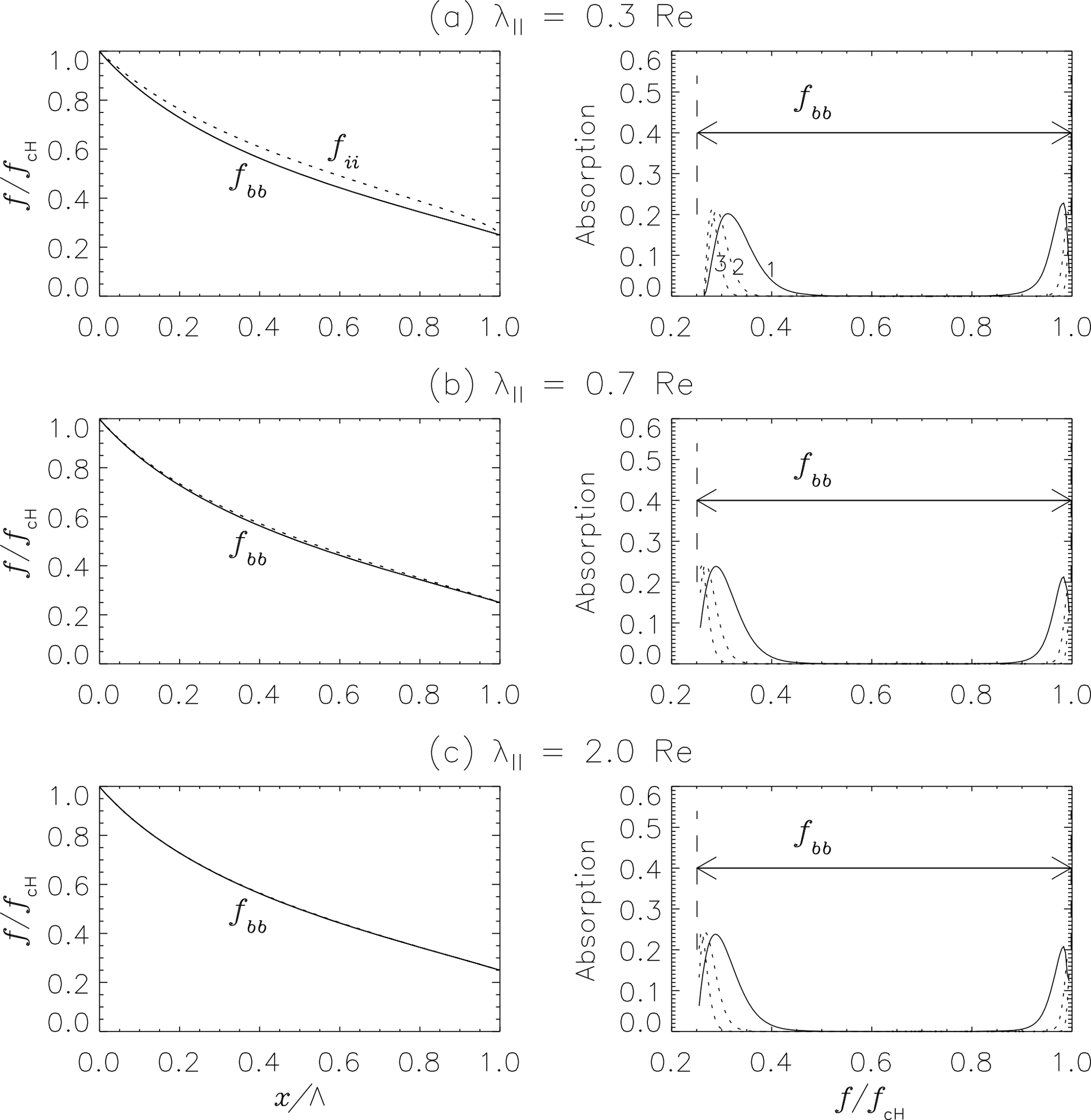
(a) λ|| = 0.3 Re
(b) λ|| = 0.7 Re
(c) λ|| = 2.0 Re
f/fcH
x/Λ
fbb
fii
Absorption
f/fcH
1
2
3

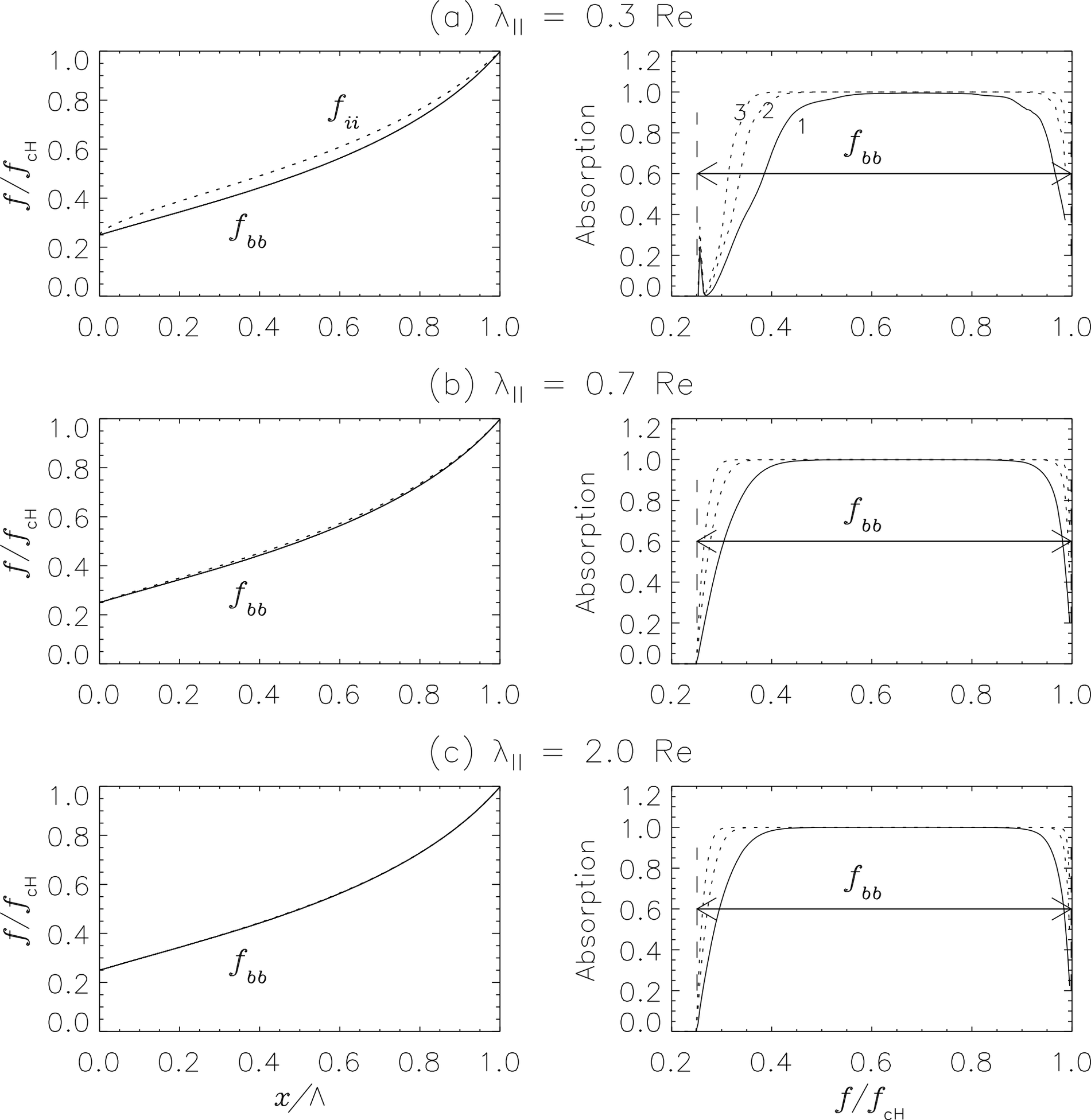
(a) λ|| = 0.3 Re
(b) λ|| = 0.7 Re
(c) λ|| = 2.0 Re
f/fcH
x/Λ
f/fcH
Absorption
fii
fbb
1
2
3

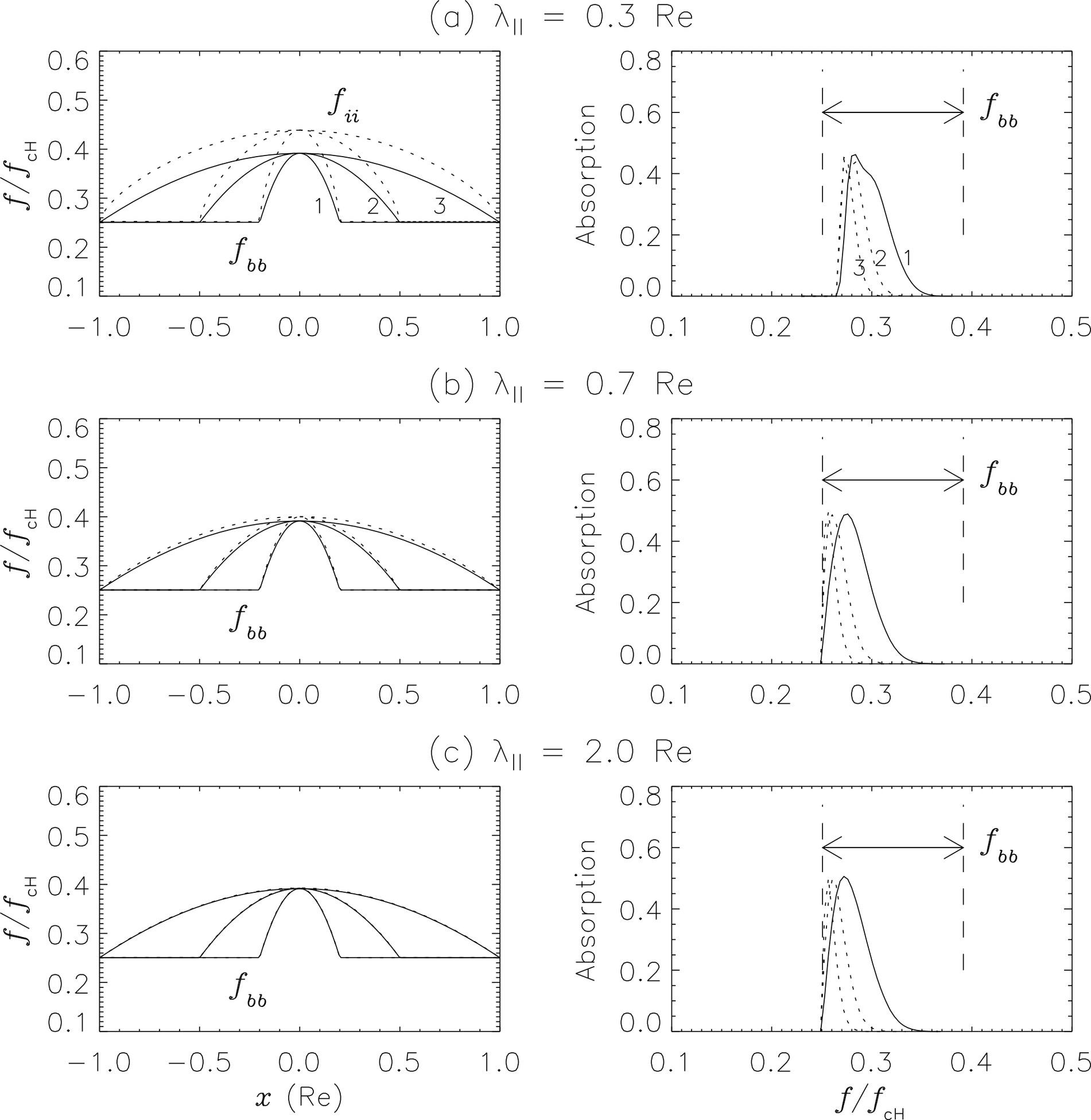
(a) λ|| = 0.3 Re
(b) λ|| = 0.7 Re
(c) λ|| = 2.0 Re
f/fcH
x (Re)
Absorption
f/fcH
fii
fbb
1
2
3

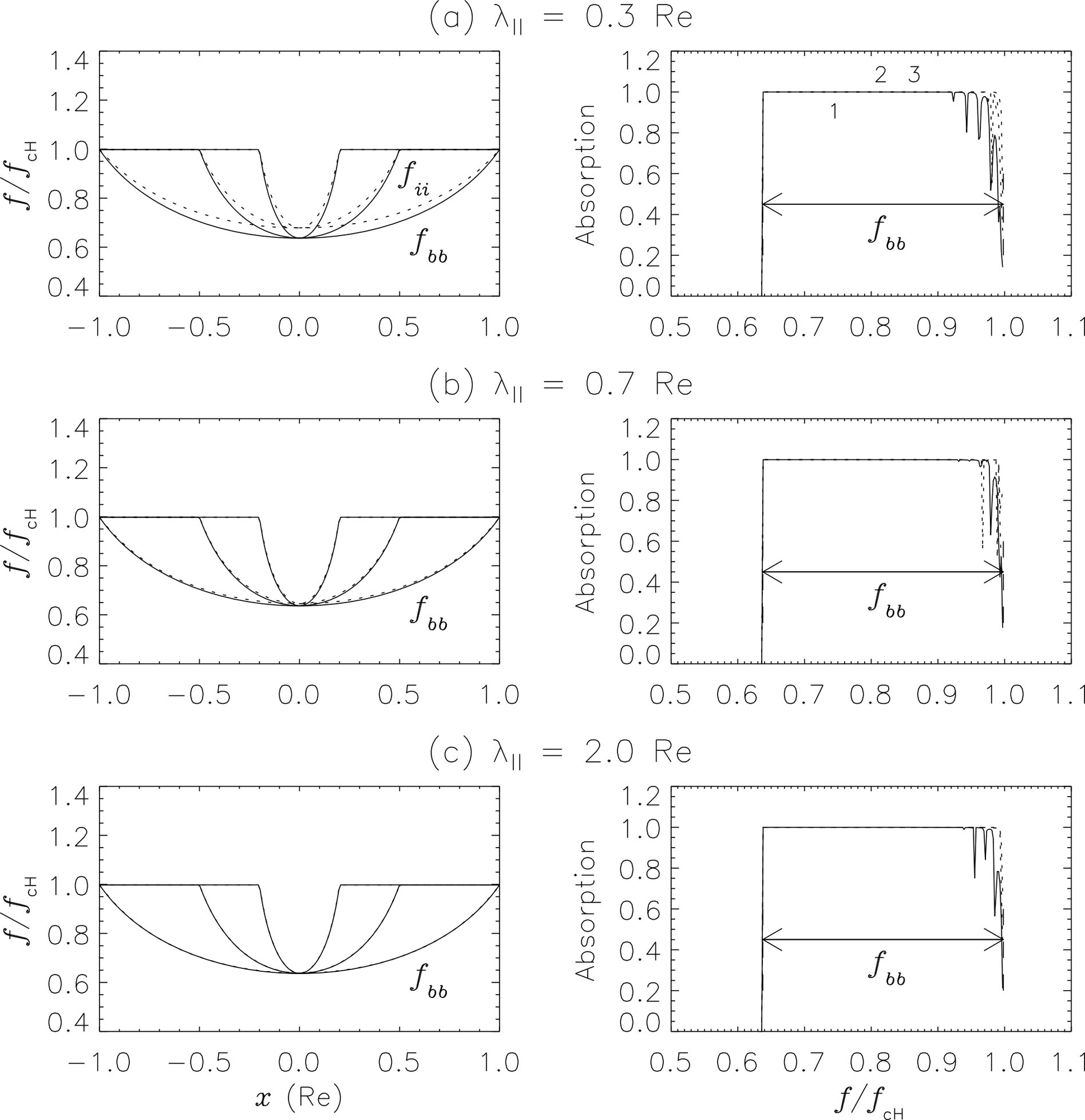
(a) λ|| = 0.3 Re
(b) λ|| = 0.7 Re
(c) λ|| = 2.0 Re
f/fcH
x (Re)
f/fcH
Absorption
fii
fbb
1
2
3

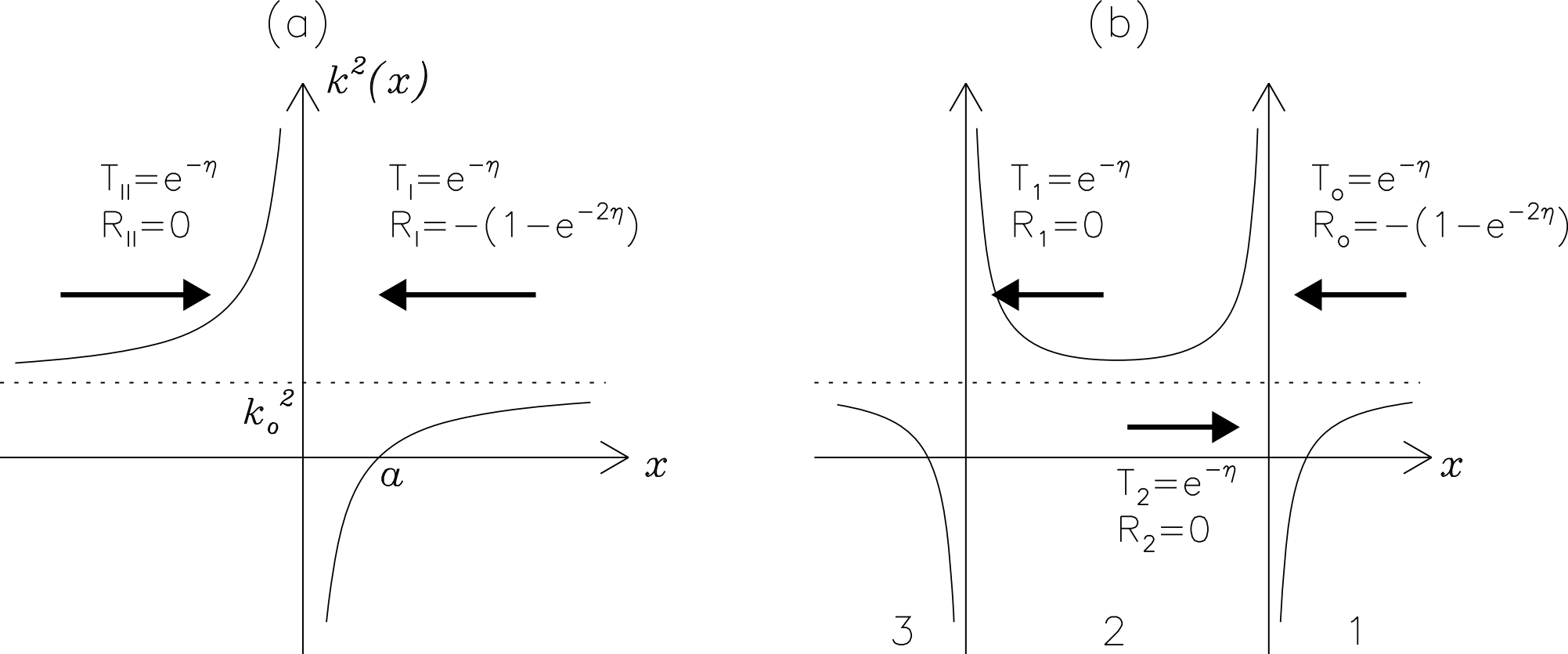
(a)
$k^2(x)$
$T_{II}=e^{-\eta}$
$R_{II}=0$
$T_I=e^{-\eta}$
$R_I=-(1-e^{-2\eta})$
$k_o^{\,2}$
a
x
(b)
$T_1=e^{-\eta}$
$R_1=0$
$T_o=e^{-\eta}$
$R_o=-(1-e^{-2\eta})$
$T_2=e^{-\eta}$
$R_2=0$
x
3
2
1

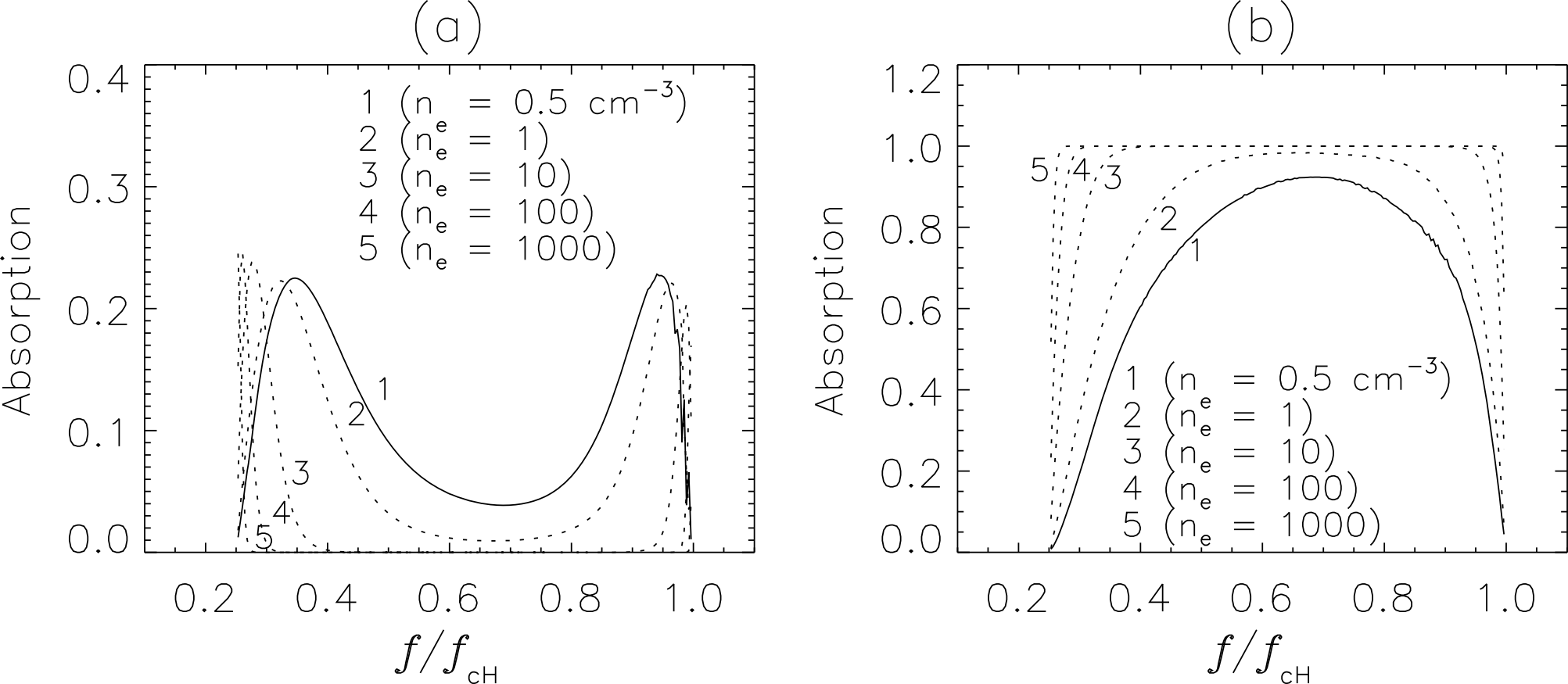
(a)
(b)
Absorption
f/f_{cH}
1 (n_e = 0.5 cm^{-3})
2 (n_e = 1)
3 (n_e = 10)
4 (n_e = 100)
5 (n_e = 1000)

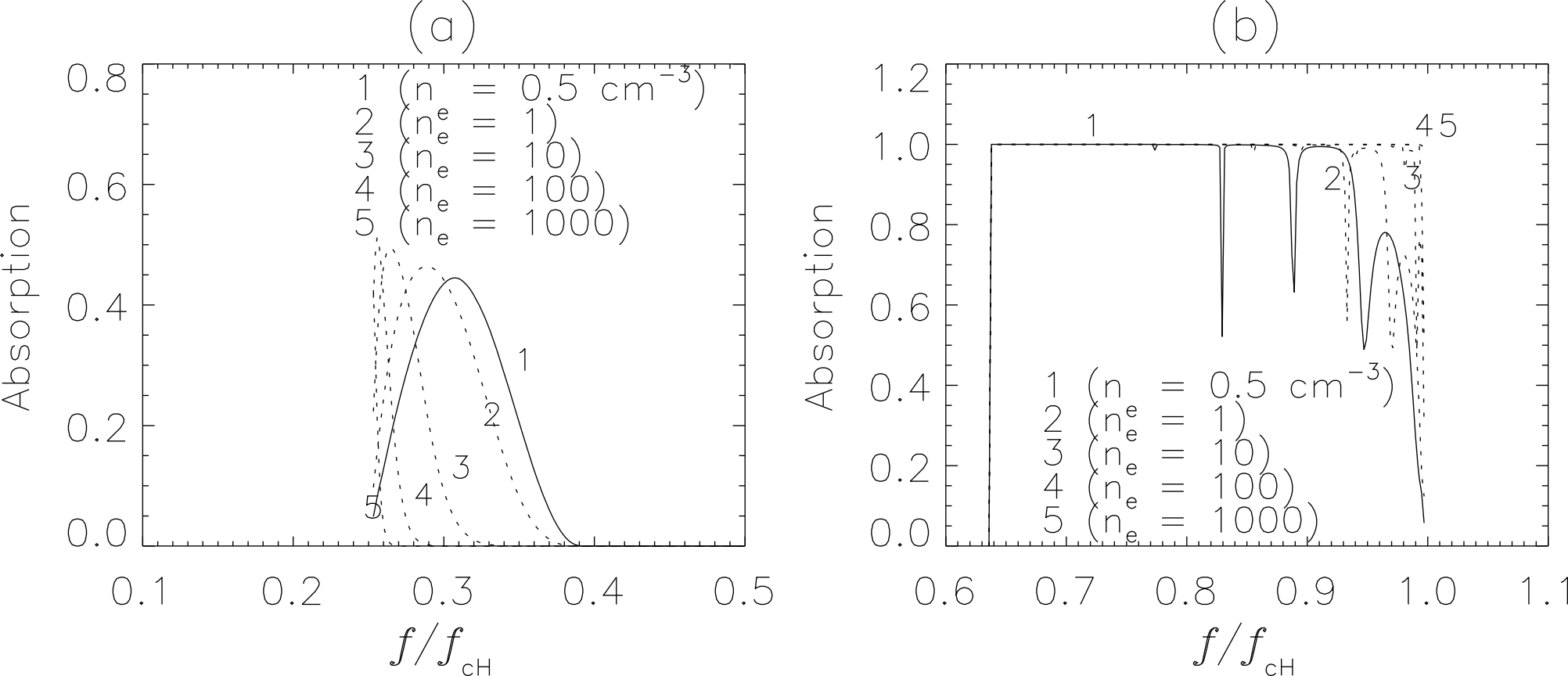
(a)
(b)
Absorption
f/f_{cH}
1 (n_e = 0.5 cm^{-3})
2 (n_e = 1)
3 (n_e = 10)
4 (n_e = 100)
5 (n_e = 1000)
0.0
0.2
0.4
0.6
0.8
1.0
1.2
0.1
0.2
0.3
0.4
0.5
0.6
0.7
0.8
0.9
1.0
1.1

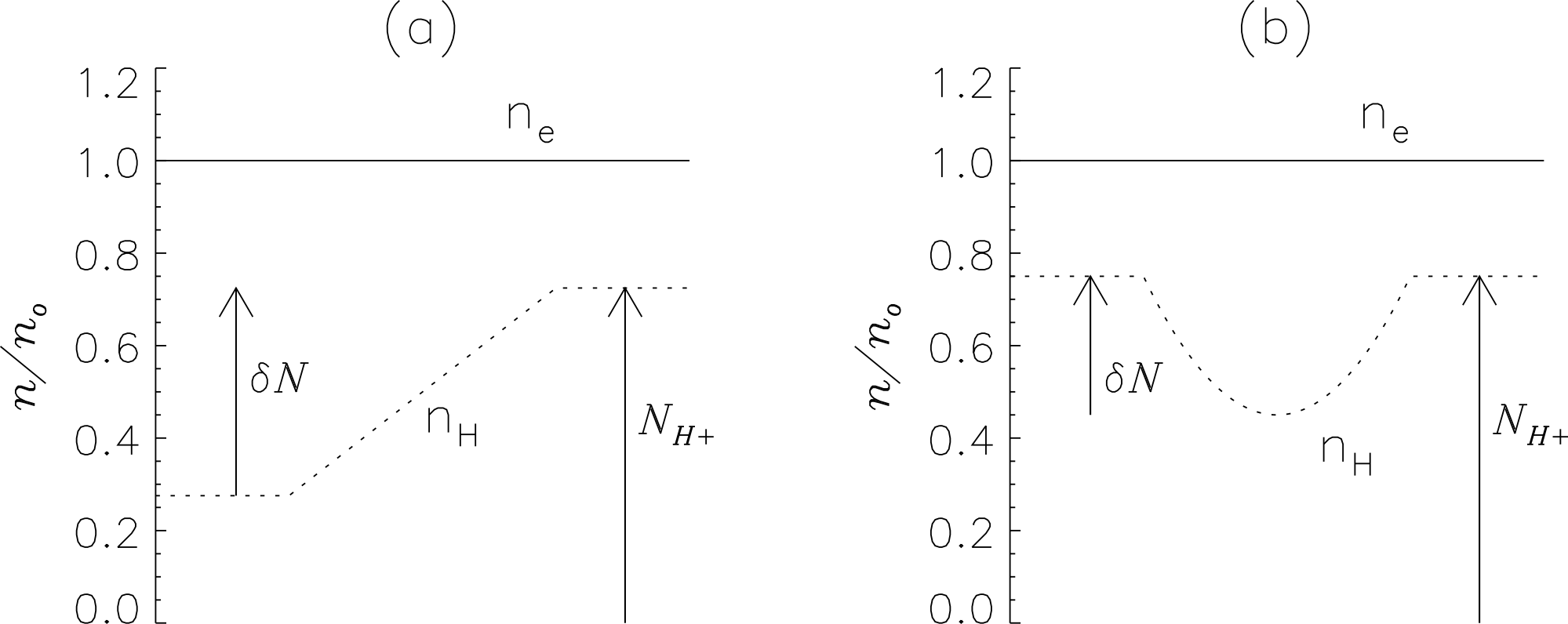
(a)
(b)
1.2
1.0
0.8
0.6
0.4
0.2
0.0
n/n_o
n_e
n_H
δN
N_{H+}

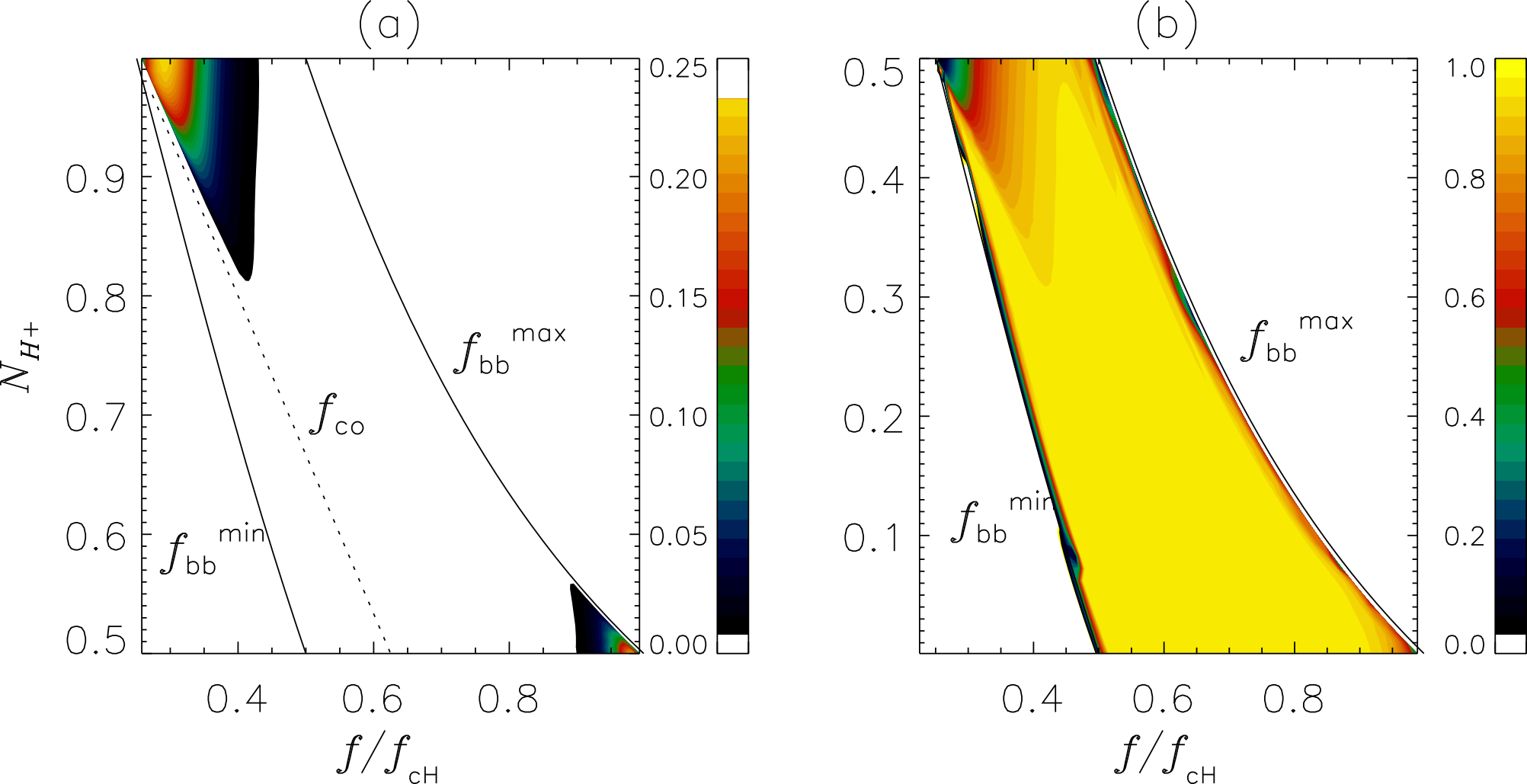
(a)
(b)
N_{H+}
f/f_{cH}
f_{bb}^{max}
f_{bb}^{min}
f_{co}
0.5
0.6
0.7
0.8
0.9
0.4
0.6
0.8
0.00
0.05
0.10
0.15
0.20
0.25
0.1
0.2
0.3
0.4
0.5
0.0
0.2
0.4
0.6
0.8
1.0

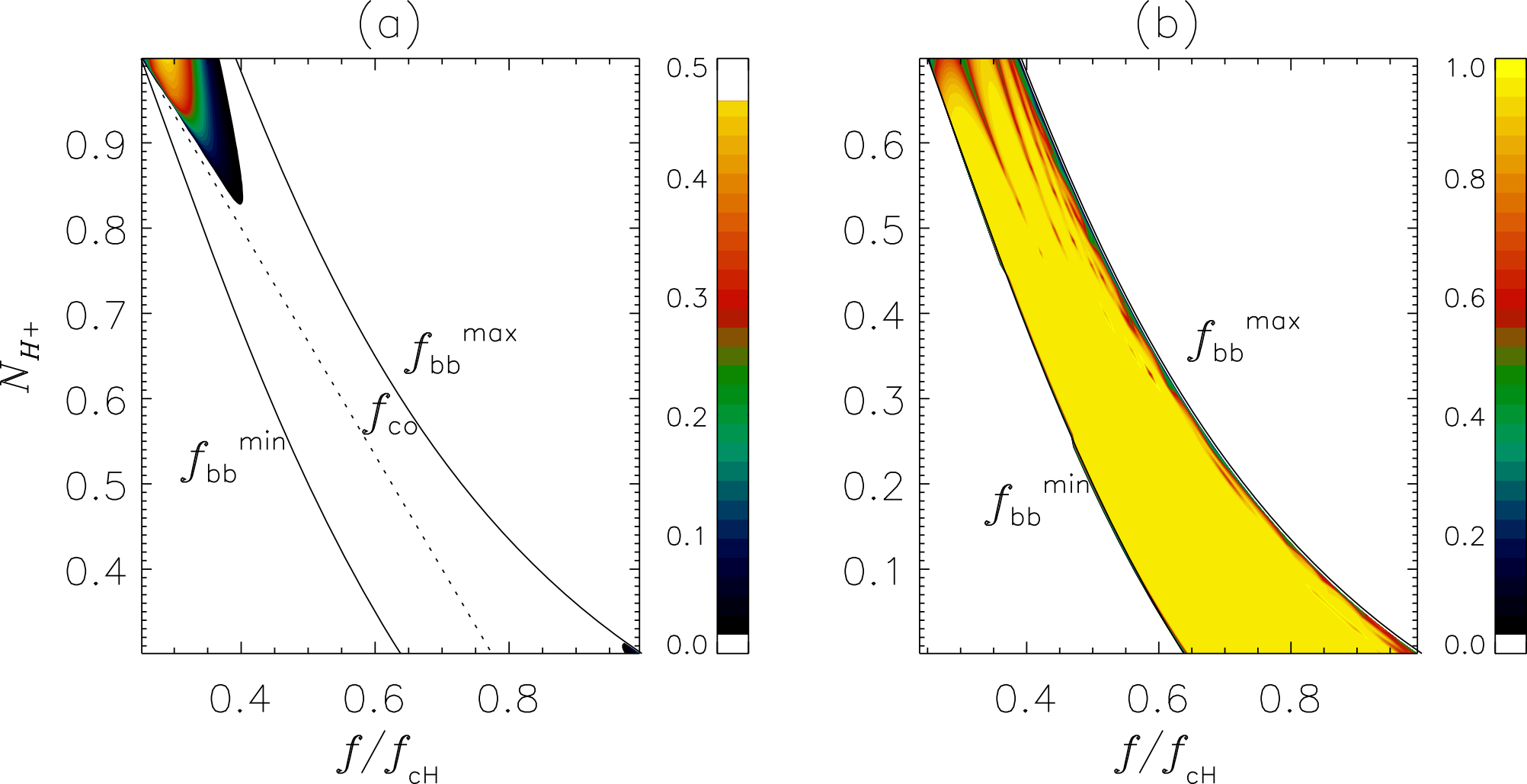
(a)
(b)
N_{H+}
f/f_{cH}
f_{bb}^{max}
f_{co}
f_{bb}^{min}
0.9
0.8
0.7
0.6
0.5
0.4
0.6
0.5
0.4
0.3
0.2
0.1
0.4
0.6
0.8
0.5
0.4
0.3
0.2
0.1
0.0
1.0
0.8
0.6
0.4
0.2
0.0

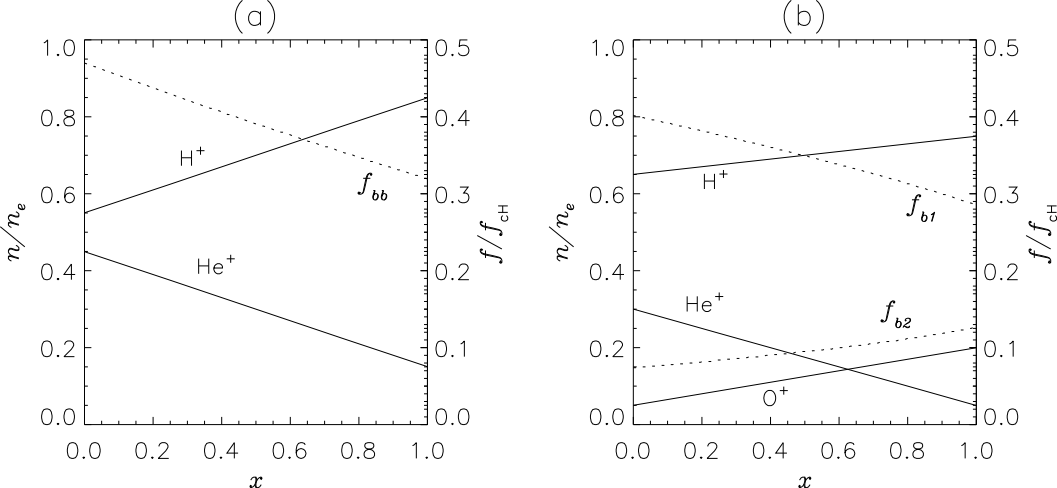
(a)
(b)
1.0
0.8
0.6
0.4
0.2
0.0
0.5
0.4
0.3
0.2
0.1
0.0
0.0
0.2
0.4
0.6
0.8
1.0
n/n_e
f/f_{cH}
x
H$^+$
He$^+$
O$^+$
f_{bb}
f_{b1}
f_{b2}

The Princeton Plasma Physics Laboratory is operated
by Princeton University under contract
with the U.S. Department of Energy.

Information Services
Princeton Plasma Physics Laboratory
P.O. Box 451
Princeton, NJ 08543

Phone: 609-243-2750
Fax: 609-243-2751
e-mail: pppl_info@pppl.gov
Internet Address: http://www.pppl.gov